Earth and Planetary Science Letters 403 (2014) 273–286

Contents lists available at ScienceDirect

Earth and Planetary Science Letters

www.elsevier.com/locate/epsl

Calculating melting temperatures and pressures of peridotite protoliths: Implications for the origin of cratonic mantle

Cin-Ty A. Lee [a,*], Emily J. Chin [a,b]

[a] Department of Earth Science, MS-126, Rice University, 6100 Main St., Houston, TX 77005, USA
[b] Geological Sciences, Brown University, 324 Brook St., Box 1846, Providence, RI 02912, USA

ARTICLE INFO

Article history:
Received 11 December 2013
Received in revised form 24 May 2014
Accepted 27 June 2014
Available online xxxx
Editor: T. Elliott

Keywords:
thermobarometer
peridotite
craton
potential temperature
lithosphere
Archean

ABSTRACT

The old, stable cores of continents – cratons – are underlain by thick and cold mantle keels, composed of melt-depleted and low density peridotite residues. The origins of these thick keels are debated. Were these thick keels formed in situ, by orogenic thickening, or by underplating of buoyant residual mantle? Key to this debate is determining the temperature and pressure at which the protoliths of cratonic peridotites melted (igneous protolith conditions) and comparing to their metamorphic (subsolidus) temperatures and pressures within the keel. This paper presents a method for explicit calculation of the temperatures and pressures at which the peridotite protoliths melted. The approach relies only on the bulk FeO and MgO of residual peridotites. A system of equations consisting of mass balance and new calibrations of Mg peridotite/melt partitioning and melt productivity is then solved simultaneously. The igneous protoliths of abyssal peridotites are found to have melted at effective pressures of 1–2 GPa and temperatures of 1300–1400 °C, within error of the magmatic temperatures and pressures of melt extraction inferred independently from the SiO_2 and MgO contents of mid-ocean ridge basalts. Archean cratonic peridotites, after filtering for the secondary effects of refertilization and orthopyroxene-metasomatism, give igneous protolith pressures and temperatures of 1–5 GPa (30–150 km) and 1400–1750 °C, similar to magmatic temperatures and pressures determined for Archean basalts thought to be representative of the thermal state of the Archean ambient mantle. Most importantly, cratonic peridotite protolith pressures and temperatures are shallower and hotter than their subsolidus equilibration pressures (3–7.5 GPa; 90–200 km) and temperatures (900–1300 °C), which reflects the recent thermal state of the cratonic lithosphere. Specifically, for individual samples with both melting and subsolidus thermobarometric constraints, we find that subsolidus pressures are 1–2 GPa (30–60 km) higher than their igneous protolith pressures although some of the deepest samples experienced minor increases in pressure. Collectively, these results support the suggestion that the building blocks of cratons were generated by hot shallow melting with a mantle potential temperature 200–300 °C warmer than the present. This shallowly generated mantle was subsequently thickened during orogenic episodes, culminating in the formation of a thick, stable craton. Whether such thickening has any modern analogs cannot be answered from this work alone.

1. Introduction

The Archean cores of continents are underlain by unusually thick and cold mantle keels, which extend to depths of 150–250 km, far exceeding the thickness of oceanic lithospheres (Pollack and Chapman, 1977; Jordan, 1978; Boyd et al., 1985, 1997; Pollack, 1986; Boyd and Mertzman, 1987; Jordan, 1988; Rudnick et al., 1998; Griffin et al., 1999, 2003; Jaupart and Mareschal, 1999; O'Reilly et al., 2001; Gung et al., 2003; Lee, 2006; Lee et al., 2011). Cold oceanic lithosphere subducts, so the thick cold thermal boundary layers underlying continents should be more convectively unstable. Yet radiogenic isotopic data seem to indicate that they have remained attached to the craton and isolated from the convecting mantle for billions of years (Walker et al., 1989; Carlson and Irving, 1994; Pearson et al., 1995a, 1995b; Carlson et al., 1999, 2005; Chesley et al., 1999; Pearson and Wittig, 2008). This has led to the suggestion that the negative thermal buoyancy of cratonic mantle is largely compensated by an intrinsic compositional buoyancy imparted by low density peridotites formed as the residues of high degrees of melt extraction (Boyd and McAllister, 1976; Jordan, 1978, 1988;

* Corresponding author. Tel.: +1 281 250 3606.
E-mail address: ctlee@rice.edu (C.-T.A. Lee).

http://dx.doi.org/10.1016/j.epsl.2014.06.048
0012-821X/

Boyd, 1989). What is not known is under what conditions these peridotite building blocks melted and how they came to form thick lithospheric keels.

The peridotites that make up most of the lithospheric mantle beneath continents have likely gone through a long and tortuous history (Kelemen et al., 1992; Herzberg, 1993; Griffin et al., 1999, 2003; Xu, 2001; Pearson et al., 2003; Herzberg, 2004; Carlson et al., 2005; Ionov et al., 2005; Lee, 2006; Ionov and Hofmann, 2007; Simon et al., 2007; Pearson and Wittig, 2008; Wittig et al., 2008; Ionov et al., 2010; Lee et al., 2011; Aulbach, 2012; Doucet et al., 2012; Herzberg and Rudnick, 2012). Before being incorporated into the upper thermal boundary layer of the Earth, peridotites from the adiabatically convecting part of the mantle start off hot. Upon decompression, they may melt and become part of the upper thermal boundary layer, eventually cooling to subsolidus temperatures (Lee et al., 2005). Depending on the tectonic environment, these peridotites may also experience changes in pressure. For example, increases in P could occur during subsequent orogenic thickening whereas decreases in P would occur with subsequent surface erosion, lithospheric thinning, or gravitational spreading of the peridotite layer. Understanding the P–T history experienced by a peridotite rock will thus have important implications for understanding how continental lithosphere forms. Does continental lithosphere form by the thickening of oceanic lithospheres, thickening of arc lithospheres, *in situ* melting in a plume head, underplating of buoyant peridotite residues, or by some other process (Helmstaedt and Schulze, 1989; Pearson et al., 1995a; Kelemen et al., 1998; Herzberg, 1999, 2004; Shirey et al., 2002; Griffin et al., 2003; Carlson et al., 2005; Cooper et al., 2006; Lee, 2006; Griffin and O'Reilly, 2007; Pearson and Wittig, 2008; Lee et al., 2011; Aulbach, 2012; Herzberg and Rudnick, 2012)?

There are already many established thermobarometers for subsolidus conditions. These include calibrations of the two pyroxene solvus, Fe–Mg exchange between pyroxene and garnet and between olivine and garnet, Al concentration in orthopyroxene coexisting with garnet, and perhaps less robust, Ni partitioning between garnet and olivine, and Cr partitioning between spinel and olivine (Ellis and Green, 1979; Harley and Green, 1982; Griffin et al., 1989; Brey and Kohler, 1990; Krogh Ravna, 2000; Wan et al., 2008). These thermobarometers give constraints on the last recorded equilibration Ps and Ts of peridotite xenoliths just before they were entrained and brought to the surface via deeply derived volcanic eruptions (Rudnick et al., 1998; Lee et al., 2011). For these reasons, the contemporary (strictly speaking, the time at which the xenoliths were erupted) thermal state of continental lithosphere is generally well constrained for many parts of the continents. By contrast, constraints on the Ps and Ts at which the igneous protoliths of peridotites melted are less robust. The challenge in estimating protolith conditions is that one cannot use the thermobarometers described above because mineral assemblages and chemistries change as P and T change. Thus, it is nearly impossible to retain the signatures of the high Ts associated with melting in the mineral assemblage unless cooling occurs rapidly, which is generally not the case for peridotites entombed within the ancient cores of continents and cooling slowly over billions of years.

Protolith melting conditions must be based on the bulk rock composition and the assumptions that the peridotite's bulk composition reflects what remained after melt was extracted and that the residual peridotite has remained a closed system in terms of mass exchange. Based on this approach, protolith Ts may be reasonably constrained. Ts are estimated from the bulk Fe and Mg contents and the T-dependency of Fe and Mg partitioning between olivine and coexisting melt (Hanson and Langmuir, 1978; Herzberg, 1992, 1999; Pearson et al., 1995b). This may seem intractable given that all thermobarometers require the composition of at least two coexisting phases to be known, but in the case of peridotites, the melt has long abandoned the peridotite residue so its composition can never be directly known. This problem was cleverly approached by taking advantage of the remarkable property that the partitioning of Fe and Mg between olivines, pyroxenes and melt is relatively insensitive to T (Hanson and Langmuir, 1978).

Current constraints on Ps of melting are more problematic. Several authors have attempted to use bulk rock Al or heavy rare earth element (HREEs) contents, reasoning that the presence of garnet during high P melting would retain Al and the HREEs more so than shallow melting in the absence of garnet (Walter, 1998, 1999, 2003; Canil, 2004; Lee, 2006; Pearson and Wittig, 2008; Lee et al., 2011). A potential complication in this approach is the growing view that many peridotites have experienced subsequent metasomatism (i.e., the assumption of closed system was violated), modifying their Al and HREE contents (as well as Fe and Mg) (Ionov et al., 2005; Simon et al., 2007; Aulbach, 2012). Only the most melt-depleted peridotites may thus be suitable for protolith thermobarometry if metasomatism is an issue. But if so, some of the most melt-depleted peridotites have melted to levels (30–50%) that would far exceed the point of garnet saturation (Bernstein et al., 2007), so low Al and HREE contents of highly melt-depleted peridotites may not be a sensitive indicator of P but rather an indicator of garnet exhaustion.

The alternative method for estimating the melting Ps and Ts of the igneous protoliths of cratonic peridotites is to examine the bulk FeO content of a peridotite (Herzberg, 1999, 2004; Ionov and Hofmann, 2007; Herzberg and Rudnick, 2012). At higher temperatures, Fe is more incompatible in the solid peridotite residuum, so bulk Fe content, as discussed above, can theoretically be used as a measure of T of melting (Pearson et al., 1995a). But given that solidus temperature increases with pressure, bulk Fe content, in conjunction with constraints from other elements, has also been used as a measure of P in several recent studies (Walter, 1998, 1999; Herzberg, 1999, 2004; Ionov and Hofmann, 2007; Herzberg and Rudnick, 2012). These studies, however, rely on graphical means of estimating P and T. Here, we build on the bulk FeO approach and provide a more quantitative means of extracting T and P.

2. Methodology

Estimating T and P requires at least two functions that relate T and P with a measurable compositional variable. One relationship is the elemental partitioning behavior between the peridotite solid residue and the melt, which depends on T and P. A second relationship involves the dependency of melt productivity on T and P, which, to first order, is controlled by the dependence of the solidus and liquidus Ts on P (Fig. 1A). That is, the amount of melt extracted from a peridotite depends on T and P. The intersection of these two equations in P–T space should, in theory, give a unique P–T of melting (Fig. 1B). However, this problem, as noted above, seems intractable because the melt that formed from this peridotite escaped long ago, so it is not possible to directly measure any partitioning relationships.

The above problem can be made tractable as follows. It is well-known that the MgO content of a melt, unlike most other elements, is buffered at a given T and P if the melt is in equilibrium with olivine (Albarède, 1992; Beattie, 1993; Herzberg and Zhang, 1996; Sugawara, 2000; Herzberg and O'Hara, 2002; Putirka, 2005, 2008; Herzberg et al., 2007; Herzberg and Asimow, 2008; Lee et al., 2009). Provided olivine is present, which is always the case during peridotite melting (at least in the uppermost mantle), the MgO content of the melt is buffered even if the composition of the bulk peridotite is not constant. To calibrate this relationship for peridotites, we used experimental melts coexisting with both olivine and orthopyroxene (valid for $P < 8$ GPa), the dominant

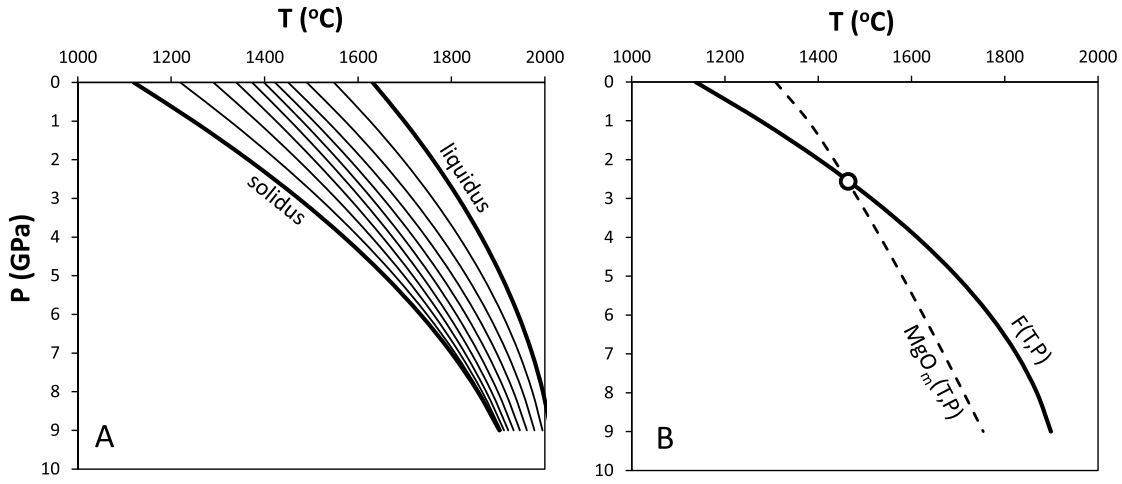

Fig. 1. A) Solidus, liquidus and melt fraction curves. B) Schematic showing how Ps and Ts of melting are estimated from peridotite residue compositions. The dashed line represents the T–P relationship for a given MgO content of the magma (MgO_m). MgO_m is estimated by mass balance as discussed in the text. The solid line represents the T–P relationship defined for a given melting fraction F. The intersection of the two lines represents the average P–T of melting experienced by the peridotite.

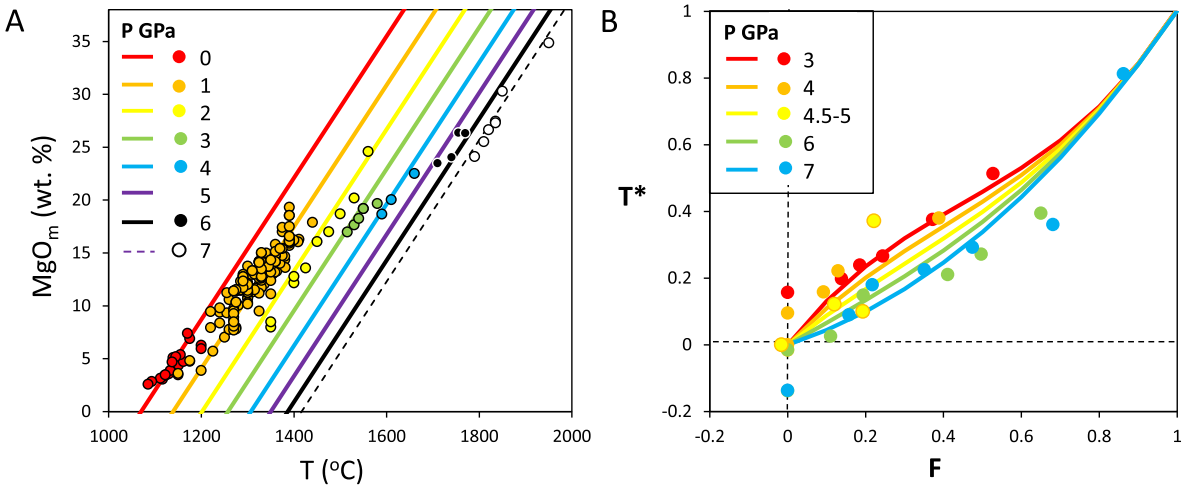

Fig. 2. A) MgO content of experimental melts (MgO_m) in equilibrium with olivine and orthopyroxene as a function of temperature. Data are color coded based on pressure of equilibration. Colored diagonal lines represent empirical calibration of MgO_m versus temperature for a given pressure (Eq. (1) in text). B) Temperature T^* (normalized to temperature interval between solidus and liquidus) versus melt fraction for batch melting of fertile peridotite using the experiments of Walter (1998). Curves represent empirical calibration of T^* versus F for different pressures (Eqs. (7) and (8)). (For interpretation of colors in this figure, the reader is referred to the web version of this article.)

mineralogy of peridotites (Stolper, 1980; Takahashi, 1980; Grove et al., 1982; Grove and Juster, 1989; Draper and Johnston, 1992; Baker et al., 1994; Gaetani and Grove, 1998; Kogiso et al., 1998; Robinson et al., 1998; Walter, 1998; Falloon et al., 1999, 2001; Falloon and Danyushevsky, 2000; Pickering-Witter and Johnston, 2000; Blatter and Carmichael, 2001; Schwab and Johnston, 2001; Bulatov et al., 2002; Pichavant et al., 2002; Grove et al., 2003; McDade et al., 2003; Wasylenki et al., 2003; Laporte et al., 2004; Parman and Grove, 2004; Feig et al., 2006). This yielded a simple empirical formula:

$$T(P, MgO_m, H_2O_m) = 1070 + 14.93MgO_m + 72.23P - 3.249P^2 - 18.53H_2O_m \quad (1)$$

where T is in Celsius, MgO and H_2O are in wt.%, and P is in GPa (Fig. 2A). This expression shows that the MgO content of a melt in equilibrium with olivine depends more on T than P. More complicated expressions for olivine-saturated thermometry exist to encapsulate a broader compositional range of basalts (Putirka, 2005, 2008), but because we are interested only in high degree melts (>10%) of peridotites, a simpler expression is sufficient. The above equation is relevant for primitive basalts and komatiites. It should not be applied to alkali-rich magmas, such as nephelinites and kimberlites.

Eq. (1) can be used to calculate a P–T relationship using only the melt composition, but as stated above, this melt composition is never known. We can, however, estimate melt MgO content by considering mass balance and mass action. Mass balance requires that

$$MgO_o = MgO_m F + (1 - F)MgO_R \quad (2a)$$

$$FeO_o = FeO_m F + (1 - F)FeO_R \quad (2b)$$

where MgO_o is the initial MgO concentration of the original unmelted peridotite, MgO_R is the measured concentration in the residual peridotite sample, and F is the integrated fraction of melt generated to form the peridotite. We assume that MgO_o and FeO_o are represented by bulk silicate Earth or primitive mantle. Melting of the mantle usually takes place by fractional melt extraction during adiabatic decompression, so that the peridotite residue experiences a range of Ts and Ps during melting. We also assume, as has been shown elsewhere, that these fractional melts pool together and that the integrated composition of the pooled melts represents an average melting T and P of the process (Herzberg,

1992, 2004; Asimow et al., 2001; Lee et al., 2009). In this regard, F also represents an average melting degree and MgO_m represents an average MgO content of the fractional melts.

Eqs. (2a) and (2b) can be related by mass action, that is, the Fe–Mg equilibrium exchange between the peridotite and the melt:

$$K_D = \frac{(FeO/MgO)_R}{(FeO/MgO)_m} = 0.381 - \frac{0.774}{MgO_m} + \frac{0.998}{MgO_m^2} \quad (3)$$

where we have used an empirical parameterization of the compositional dependence of K_D (Herzberg and O'Hara, 2002). Because MgO_m depends on T, as shown in Fig. 1, Eq. (3) effectively accounts for any T dependencies of K_D. Combining the mass balance equations (2a) and (2b) with Eq. (3) allows elimination of F, which gives an expression for the MgO of the melt, MgO_m

$$MgO_m = \frac{FeO_R(MgO_R - MgO_o) - MgO_R(FeO_R - FeO_o)}{(FeO_o - FeO_R) + (MgO_R - MgO_o)(FeO_R/MgO_R)/K_D} \quad (4)$$

as a function of known quantities (MgO_R, FeO_R, MgO_o, FeO_r). Because K_D depends explicitly on MgO_m, one must solve for the root of Eq. (4) to obtain MgO_m. Plugging Eq. (4) into Eq. (1) leads to an isopleth of MgO_m in P–T space. We have resolved the issue of not having a melt to directly measure, but we are still left with a relationship between P and T.

A second constraint relates T, P and F, the latter of which comes from solving the above system of equations. We first define a quantity T^*, which represents the T *normalized* to the T difference between the P-dependent solidus ($T_S(P)$) and liquidus ($T_L(P)$)

$$T^*(P) = \frac{T(P) - T_S(P)}{T_L(P) - T_S(P)} \quad (5)$$

T_L is equivalent to the T of a magma having a composition equivalent to the bulk starting mantle, and thus, is calculated for any given starting composition by substituting MgO_o for MgO_m in Eq. (1). For T_S, we assume a mantle solidus from Hirschmann (valid for $P < 10$ GPa) corresponding to that for the primitive upper mantle ($MgO_o = 37.8$, $FeO_o = 8.05$, $Na_2O + K_2O = 0.39$, $Al_2O_3 = 4.45$ wt.%; McDonough and Sun, 1995) (see Fig. 1A)

$$T_S(°C) = 1120 + 132.9P - 5.104P^2 \quad (6)$$

We then use a polynomial parameterization of T^* versus F:

$$T^* = a_1F + a_2F^2 + a_3F^3 \quad (7)$$

where the constants are allowed to depend on P (GPa). To determine the constants, we used the experimental data of Walter, which are based on a West Kettle River peridotite as shown in Fig. 2A (Walter, 1998, 1999). We note that Walter's solidus T for the West Kettle River peridotite is 30° lower than that given by Eq. (6) (Hirschmann, 2000). To calibrate Eq. (7), we thus shifted the solidus and liquidus T at 1 atm in Eq. (6) down by 30°, assuming that the functional relationship of T^* does not change. This yielded the constants for Eq. (7) (Fig. 2B):

$$a_1 = 2.288 - 0.271P \text{ (GPa)}$$
$$a_2 = -3.474 + 0.572P$$
$$a_3 = 2.195 - 0.302P \quad (8)$$

We now have a set of equations that can be solved simultaneously for T, P, MgO_m and F. These are $T(F,P)$, $T(P,MgO_m)$, MgO_m and $F(MgO_m)$. We note that although Eq. (1) accounts for H_2O, we have not included the effects of H_2O on the parameterizations of T, F and P. H_2O will decrease T_S and thereby increase T–T_S and change the functional form of $T^*(F)$. Incorporating the effects of

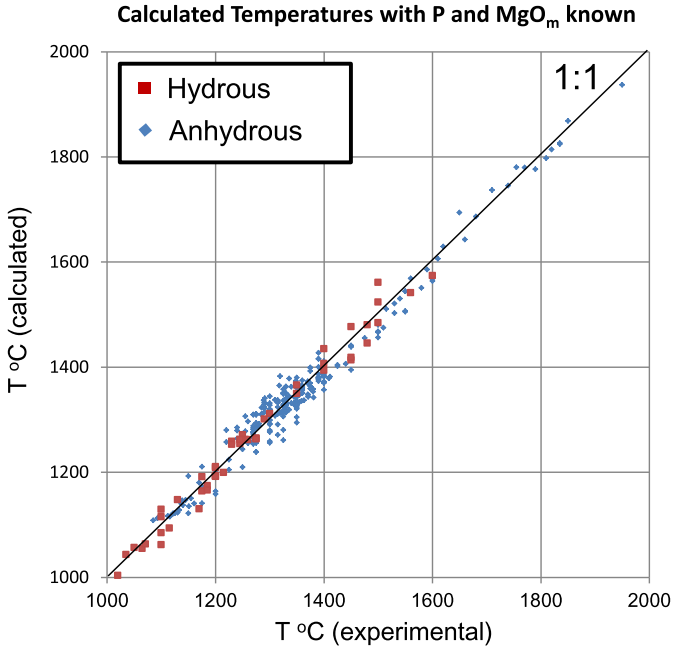

Fig. 3. Temperatures calculated from the MgO content of experimental melts in equilibrium with coexisting olivine and orthopyroxene versus experimental temperatures. The solid line represents the 1:1 correspondence line.

H_2O (or other volatiles, such as CO_2) is beyond the current scope of this paper, so all calculations here assume anhydrous systems. An Excel spreadsheet is provided, along with instructions, to help the reader make these calculations.

3. Accuracy, precision and relevance to natural processes

Precision is evaluated by how well experimental T is reproduced from Eq. (1) using melt composition with experimental P known (Fig. 3). In this ideal case, uncertainties in T are less than 20 °C. A more relevant evaluation of precision is to treat experimental data as we would treat natural data, that is, when both T and P are unknown. For natural samples, only FeO_R and MgO_R are used. We thus take the experimental FeO_R and MgO_R of Walter (1998) and solve for P, T, F and MgO_m (Fig. 4). Provided we assume a lower solidus T for Walter's bulk rock peridotite composition (1090 °C instead of 1120 °C at 1 atm), as discussed above, we reproduce experimental quantities as follows: <5% for T, <0.7 GPa for P, <10% for F, and <5% for MgO_m. We consider these uncertainties to be the nominal internal uncertainties in our calculations for natural samples.

Accuracy is much more difficult to evaluate because it depends on how representative the experimental data are. The number of high pressure (>3 GPa) melting experiments used to calibrate the thermobarometric equations are primarily from Walter (1998) and thus depend on the accuracy of those experiments. Accuracy can also be compromised by uncertainties in the bulk composition of residual peridotites and assumed primitive mantle composition. These and other accuracy issues are discussed in more detail in Section 4.5.

As for applicability to natural samples and processes, our estimated T–Ps should correspond to the exact T–P of melting under isobaric batch melting conditions, as shown by the ability of the method to reproduce the P–Ts of experiments, which are inherently performed under batch conditions. On the other hand, if melting occurs by polybaric fractional melting during adiabatic decompression, as is generally thought to be the case, melts are generated over a range of T–P and the meaning of the calculated P–T becomes less clear. We assume that T-Ps estimated using our

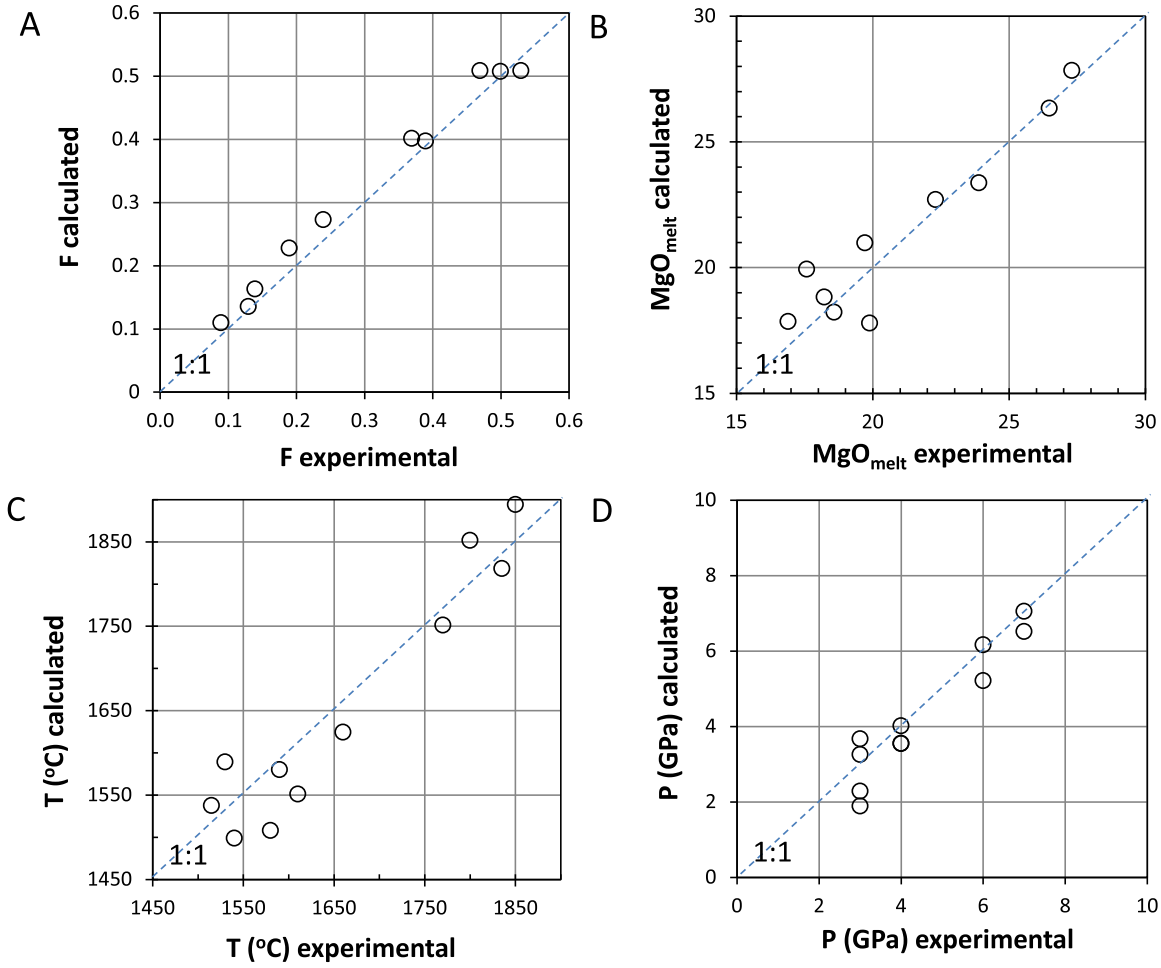

Fig. 4. A) Melting degree (F), B) MgO content of the melt (MgO_m), C) T (Celsius) and D) P (GPa) of peridotite melting experiments of Walter (1998) calculated using only the MgO and FeO contents of the peridotite residue. Dashed lines correspond to 1:1 correspondence lines between calculated and experimental values. In calculating these quantities for Walter's experiments, a solidus T of 1090 °C was used to account for the lower melting points reported in Walter (1998).

proposed method represent the average P–T of the polybaric melting column, in which case the estimated Ps and Ts are maximum bounds on the final Ps and Ts experienced by the decompressing peridotite.

4. Application to real peridotites

4.1. Filtering for open-system processes

Applying the method to real samples requires exclusion of those samples that may have been chemically modified since their formation, at least in terms of major elements like Fe and Mg. This can be seen in Fig. 5, where we plot bulk MgO versus FeO for peridotites along temperature and melt fraction contours calculated for 1 and 2.5 GPa. At a given P, high T depletes the residue in Fe significantly. It can also be seen that high Ps also result in Fe depletion (Fig. 5B). These T–F contours at a given P should not be used to estimate P–Ts of the peridotite protolith because we have assumed P to be constant. However, these figures allow one to evaluate some of the effects associated with open system processes.

Some cratonic peridotites are thought to have experienced secondary orthopyroxene-enrichment, which has the effect of increasing SiO_2 while decreasing bulk FeO and MgO, causing T and P to be over-estimated (Boyd, 1987, 1989; Herzberg, 1993; Rudnick et al., 1994; Kelemen et al., 1998; Lee et al., 2003, 2011; Lee, 2006; Aulbach, 2012). The orthopyroxene effect, however, can be filtered by excluding those samples with anomalously high SiO_2 for a given Mg# (atomic Mg/(Mg + Fe)), which does not change during orthopyroxene-enrichment. We define here the following criteria to identify samples unmodified by orthopyroxene-enrichment:

$$(\mathrm{Mg}+\mathrm{Fe})/\mathrm{Si} > -82.814\mathrm{Mg}\#^2 + 160.6\mathrm{Mg}\# - 76.05 \quad (9)$$

where all elements are in units of atomic fraction (this equation was derived here from a plot of atomic (Mg + Fe)/Si versus Mg# as shown in Lee et al., 2011). This equation identifies orthopyroxene-rich samples as those having anomalously high SiO_2 content using the property that orthopyroxene has an atomic (Mg + Fe)/Si of ~1 and olivine a value of 2.

It has also been suggested that fertile to moderately depleted peridotites may have once been more depleted but have subsequently been metasomatized by the addition or passage of basaltic melts. Such processes could modify Fe and Mg contents, resulting in spurious T and P estimates (Fig. 5). To avoid refertilization effects for cratonic peridotites, we apply our calculations to peridotites with Mg#s $\geq$ 0.92. For abyssal peridotites, we use only those samples with Mg#s $>$ 0.905 because few samples exceed 0.91.

Finally, weathering and serpentinization can dilute or enhance absolute elemental concentrations. We thus avoid samples that have low metal-oxide totals (<96 wt.%). We then normalize metal oxide concentrations to 100%.

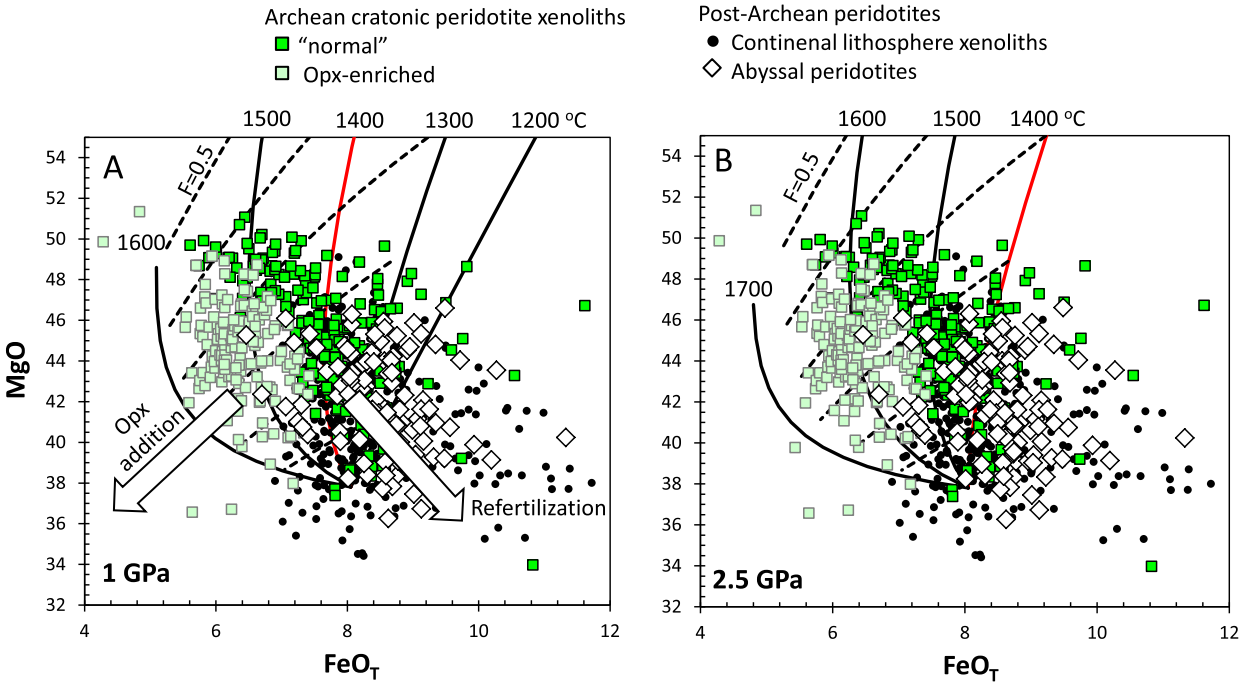

Fig. 5. MgO versus FeO in the solid residuum, where FeO_T represents all Fe taken as FeO. Data represent peridotites from Archean cratons (xenoliths), Phanerozoic continents (xenoliths), and abyssal peridotites. Cratonic peridotites have been subdivided into orthopyroxene-enriched and "normal" peridotites according to the criteria outlined in the text. Solid lines represent isothermal melt depletion curves. The red line represents the 1400 °C isotherm. Two figures have been calculated to show that the partitioning of MgO between peridotite and melt depends on assumed P. Thus, the absolute Ts shown in any given plot are not unique unless P is also known. The purpose of this figure is primarily to show the effects of secondary metasomatic processes. Arrows showing the effects of orthopyroxene-enrichment and refertilization are denoted. (For interpretation of the references to color in this figure legend, the reader is referred to the web version of this article.)

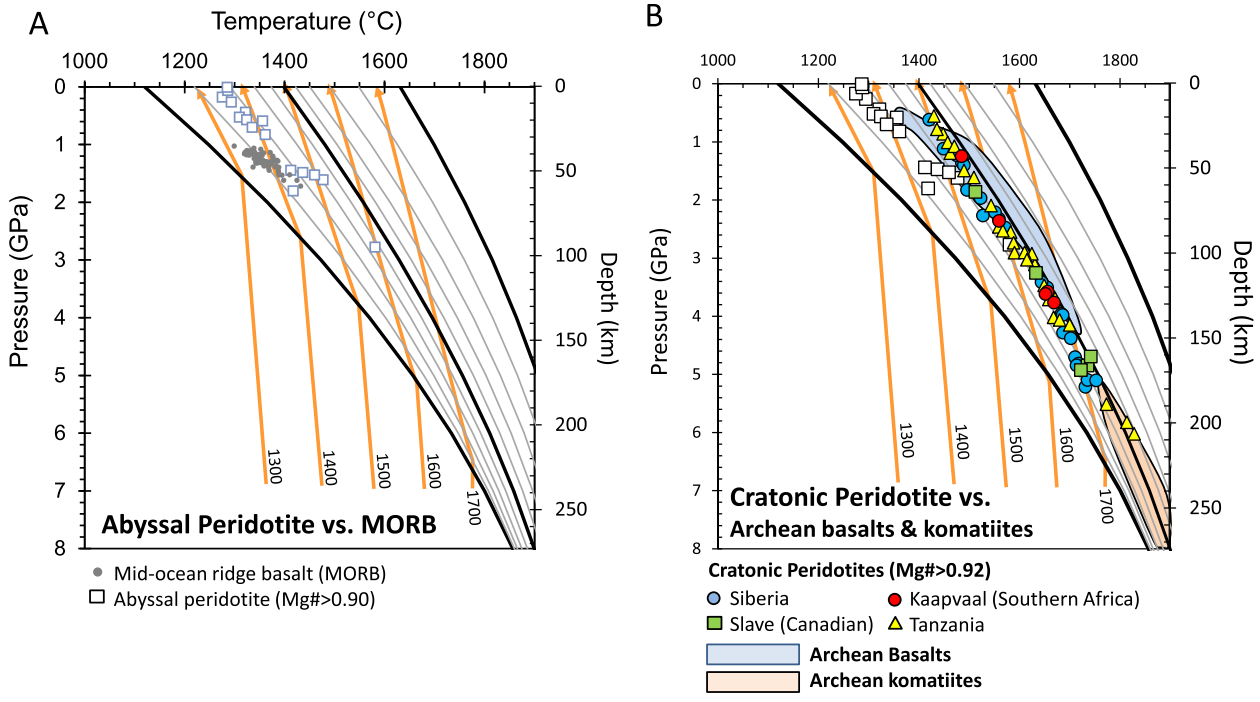

Fig. 6. A) P–T plot comparing melting conditions inferred for abyssal peridotites (this study) and mid-ocean ridge basalts (Lee et al., 2009). B) Comparison of melting conditions for Archean cratonic peridotites (this study) and Archean komatiites (Herzberg et al., 2010). Orange lines represent solid and melting adiabats (Iwamori et al., 1995). Curved lines represent the solidus, liquidus and constant melt fraction contours for primitive mantle using the parameterizations described in the text. (For interpretation of the references to color in this figure legend, the reader is referred to the web version of this article.)

4.2. Abyssal peridotites from modern ocean basins

Melting Ts and Ps were calculated for abyssal peridotites with Mg#s >0.905 from Niu's database (Niu, 2004). Abyssal peridotites are thought to represent residual peridotites associated with the generation of mid-ocean ridge basalts, so we use these rocks as representative of Phanerozoic conditions. Ts and Ps range from 1300 to 1400 °C and 0.5 to 1.5 GPa and melting degrees F of ~20% are obtained (Fig. 6A). We note that some negative, and clearly erroneous, Ps are also calculated (not shown) for samples with

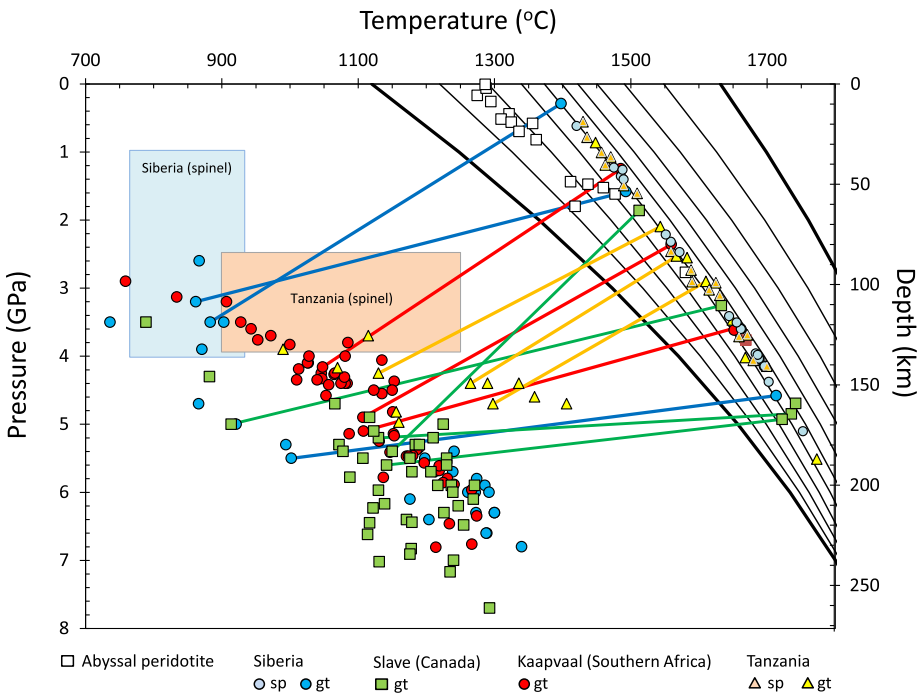

Fig. 7. P–T plot for cratonic peridotites showing both igneous protolith (this study) and metamorphic/subsolidus conditions based on two pyroxene thermometry and garnet–orthopyroxene barometry (see text). Tie lines connect protolith and metamorphic Ps and Ts for those samples in which both types of P–Ts could be calculated. Calculations for cratonic peridotites are shown only for peridotites with Mg# $>$ 0.92 and no orthopyroxene-enrichment. Curved lines represent the solidus, liquidus and constant melt fraction contours described in the text. Note that some cratonic peridotites (Tanzania and Siberia) have been subdivided into spinel and garnet peridotites. Subsolidus pressures cannot be calculated reliably for spinel peridotites, but approximate subsolidus P ranges for spinel peridotites can be calculated by comparing T constraints with apparent geotherms defined by garnet-bearing peridotites.

unusually high FeO ($>$10 wt.%), which we discuss in Section 4.5. Ignoring such samples, the abyssal peridotites are slightly higher than the average Ts and Ps of melting estimated from mid-ocean ridge basalts using independent Mg-based thermometers (Putirka, 2005; Herzberg et al., 2007; Lee et al., 2009) and Si-based barometers (Lee et al., 2009) as shown in Fig. 6A. It is not clear, however, if this difference is significant given uncertainties in magma thermobarometry and the present peridotite thermobarometry. In the case of magma thermobarometry, there is potentially a 50–100 °C uncertainty due to uncertainties in estimating the primary magma composition. In the case of the abyssal peridotites, Fe and Mg contents may be modified by serpentinization. In any case, abyssal peridotite melting Ts and Ps are consistent with a mantle potential temperature between 1300 and 1450 °C.

4.3. Cratonic peridotites

We now turn to the cratonic peridotites that make up the thick mantle keels underlying most Archean cratons. We examine peridotite samples from the Siberian (Boyd et al., 1997; Ionov et al., 2010; Doucet et al., 2012), Slave (Kopylova et al., 1998, 1999a, 1999b; Kopylova and Russell, 2000; Aulbach et al., 2004), South African (Simon et al., 2007; Gibson et al., 2008) and Tanzanian cratons (Rudnick et al., 1994; Lee and Rudnick, 1999; Gibson et al., 2013). With this dataset, we present igneous protolith T–Ps for garnet-bearing and garnet-free (mostly Tanzania and Siberia) peridotites. We show the subsolidus (metamorphic) equilibration Ts and Ps for the same samples based on the pyroxene and garnet thermobarometry reported in the above cited studies. For spinel peridotites, we are unable to provide precise subsolidus P–T estimates, but can provide approximate P–T fields based on an upper pressure bound defined by the spinel garnet transition (O'Neill, 1981) and a low pressure bound defined by crustal thickness (~45 km). Some estimates of the subsolidus pressures of spinel peridotite xenoliths can also be inferred by combining temperature constraints with extrapolations of apparent geotherms defined by the thermobarometric constraints of garnet-bearing peridotites (cf. Lee and Rudnick, 1999). Subsolidus T–Ps represent the thermal state of the lithosphere just prior to entrainment of the xenoliths in kimberlites, all of which are Phanerozoic in age. Igneous protolith P–Ts record melt extraction events, which, based on Re–Os isotope systematics, indicate that most of these cratonic peridotites melted during the Archean (Pearson et al., 1995a, 2003; Carlson et al., 1999, 2005; Pearson and Wittig, 2008). Tie lines connecting metamorphic and igneous protolith T–Ps are drawn for those samples in which sufficient data exists and define the initial and "final" states of cratonic peridotites.

It can be seen from Fig. 6B that cratonic peridotites melted between 1400 and 1750 °C over Ps between 0.2 and 6.2 GPa, corresponding to melting degrees F of 30–50%. These T–Ps range to significantly higher values than that inferred above for abyssal peridotites, indicating that the cratonic peridotites were formed by hotter and deeper melting. Mantle potential temperatures required to form the cratonic peridotites appear to range from ~1500 to 1700 °C. Metamorphic T–Ps, by contrast, range between 900 and 1300 °C and 3 and 7.5 GPa, and thus record colder and deeper conditions than their igneous protoliths (Fig. 7). Tie lines connecting metamorphic and igneous T–Ps for the same sample (Fig. 7) show that many of the peridotites have experienced an increase in P since their formation, ranging from a small change in P ($<$0–1 GPa) in the deepest samples to $<$2 GPa for shallower samples. If these peridotites melted by decompression melting, then the estimated Ps are maximum bounds on the final Ps to which the peridotites ascended during melting, which would imply even greater increases in P experienced by the peridotites since the formation of their protoliths.

Our results are consistent with previous suggestions, based primarily on graphical interpretations of elemental variation diagrams, that cratonic peridotites have experienced an increase in

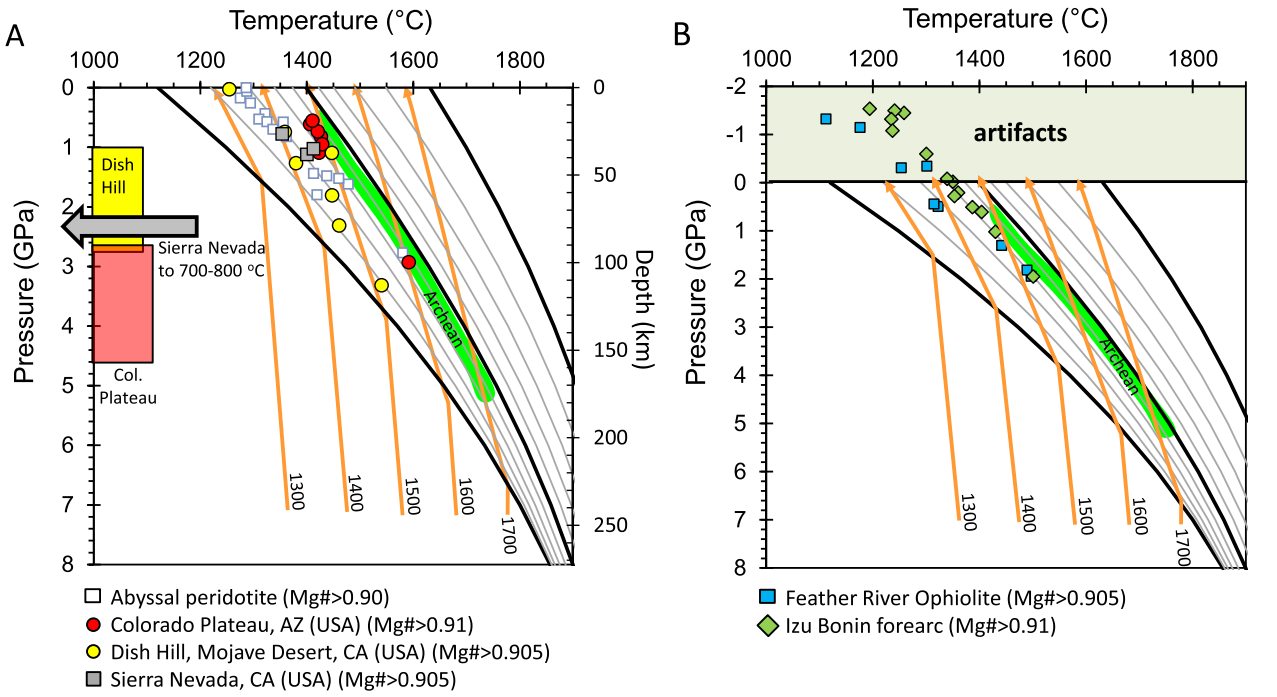

Fig. 8. Same as in Fig. 7, but for post-Archean peridotites. A) Igneous protolith P–Ts of peridotites from western North America (symbols) along with fields showing range of subsolidus P–Ts. B) Igneous protolith P–Ts of fore-arc and ophiolitic peridotites. Note that some samples give negative Ps, which are clearly erroneous and hence labeled as "artifacts". Such under-estimation of P (and T) could be related to Fe-metasomatism and/or serpentinization (see Fig. 9). Green arrays in A) and B) represent igneous protolith P–T_S of Archean cratonic peridotites from Fig. 7. All other curves as in Fig. 7. (For interpretation of the references to color in this figure legend, the reader is referred to the web version of this article.)

P since their formation as melt residues (Saltzer et al., 2001; Canil, 2004; Lee, 2006; Ionov and Hofmann, 2007; Pearson and Wittig, 2008; Lee et al., 2011; Doucet et al., 2012). Our calculated melting Ts of the protoliths are consistent with other estimates of peridotite melting T (Herzberg, 2004; Lee et al., 2011; Herzberg and Rudnick, 2012).

We can also compare cratonic peridotite melting Ts and Ps to those calculated for Archean basalts and komatiites (Fig. 7) based on thermobarometric constraints published elsewhere (Herzberg et al., 2010; Herzberg and Rudnick, 2012). Although there are uncertainties in magma thermobarometry, as discussed above for mid-ocean ridge basalts, it appears that cratonic peridotites melted at conditions similar to those of Archean basalts, that is, at potential temperatures between 1500 and 1700 °C. Komatiites, however, appear to have formed at potential temperatures greater than 1700 °C, which would suggest that cratonic peridotites and komatiites might not be complementary.

4.4. Post-Archean mantle

We have also examined post-Archean continental lithospheric mantle xenoliths from the Colorado Plateau (The Thumb, Arizona), the Mojave Province (Dish Hill, California), and the Sierra Nevada batholith (California) in western USA (Ehrenberg, 1982; Lee et al., 2001b; Luffi et al., 2009; Chin et al., 2012, 2014). The Colorado Plateau xenoliths, based on Re–Os isotopic systematics, are thought to be mid-Proterozoic in age (Lee et al., 2001b) and are represented by garnet peridotites derived from depths of 3–4.5 GPa (100–150 km) (Riter and Smith, 1996; Smith, 2000; Li et al., 2008). The Mojave Province xenoliths from Dish Hill are spinel peridotites (<3 GPa or <90 km depth), which have been interpreted to represent subcreted Farallon oceanic lithosphere (Luffi et al., 2009), although recent Re–Os isotope studies hint that there may be some component of Paleo- to Mid-Proterozoic lithospheric mantle (Armytage et al., 2014). Most of the Sierra Nevada peridotites are interpreted to represent juvenile mantle associated with the formation of the Sierran continental arc batholith during the Cretaceous (Lee et al., 2000, 2001a; Chin et al., 2012) and, at the time of xenolith sampling (~8 Ma; Dodge et al., 1988), the xenoliths derived from pressures between 2 and 3 GPa (60–90 km) at relatively cool (700–800 °C) temperatures (Mukhopadhyay and Manton, 1994; Ducea and Saleeby, 1996, 1998; Lee et al., 2001a; Chin et al., 2012).

Protolith Ps and Ts are shown in Fig. 8A. Only peridotites with Mg# > 0.905 were used for the Sierran and Mojave samples and >0.91 for the Colorado Plateau samples. It can be seen that the Mojave and Sierran peridotites, for the most part, have igneous protolith Ps and Ts indistinguishable from "modern" abyssal peridotites. These samples give significantly lower igneous protolith Ts, Ps, and melting fractions F then Archean cratonic peridotites. The Sierran and Mojave peridotites are consistent with mantle potential temperatures between 1300 and 1450 °C. The Colorado Plateau peridotites yield higher Ts and overlap with the shallow end of the Archean cratonic peridotite array, but suggest a mantle potential temperature of ~1500 °C, which is less than the range observed for Archean peridotites (1500–1700 °C). For the Sierran and Colorado Plateau peridotites, final subsolidus equilibration Ps are higher than their igneous protolith Ps.

We have also examined dredged fore-arc peridotites (Mg# > 0.91) from Izu–Bonin (Parkinson and Pearce, 1998) and ophiolitic peridotites (Mg# > 0.905) from the Feather River Ophiolite complex in the western Sierra Nevada, California, USA (Li and Lee, 2006). These peridotites yield low Ps and Ts and high melting degrees (Fig. 8B). Temperatures are slightly higher than that of abyssal peridotites. We note that many of the samples give negative Ps. All of these peridotites have been serpentinized to some extent, which could increase Mg contents (relative to Fe), leading to under-estimation of P and T (see Section 4.5). It is also possible that these peridotite residues melted under water-rich

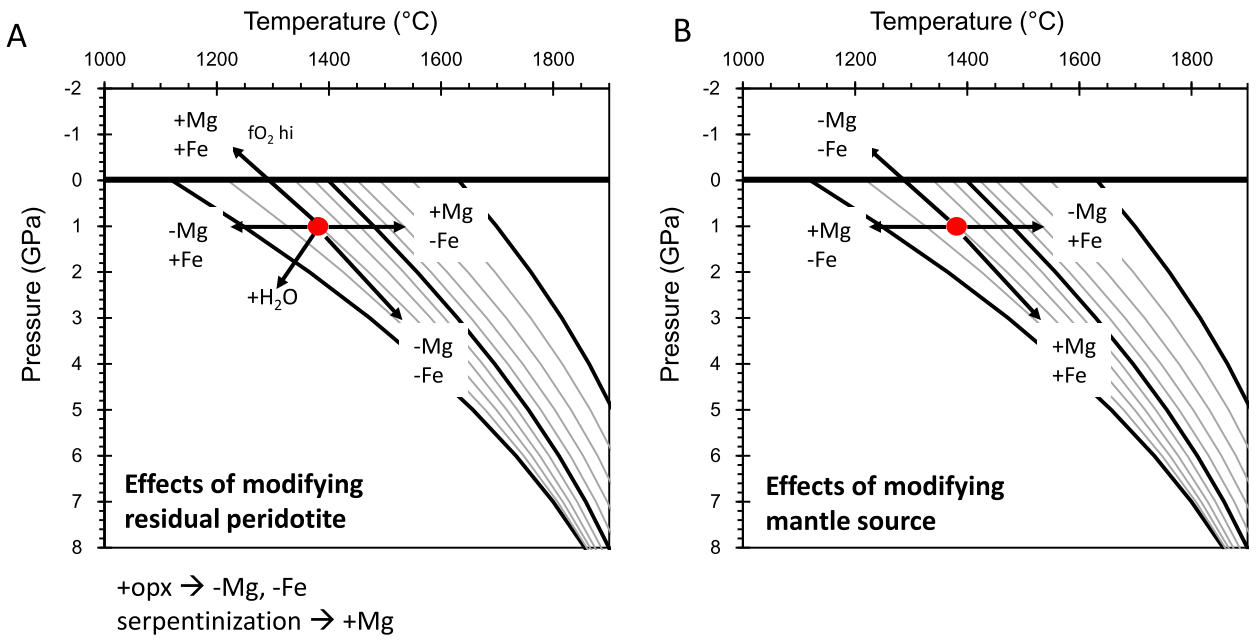

Fig. 9. This diagram shows P–T artifacts associated with uncertainties in the original bulk composition of the peridotite residue (A) and mantle source (B).

conditions. As discussed below, failure to account for water would cause under-estimation of P and over-estimation of T.

4.5. Caveats and potential pitfalls

As with any thermobarometer, our method comes with potential sources of systematic error. The validity of the entire method rests on key assumptions. We list these assumptions below and show in Fig. 9 how they translate into potential errors in P–T. The reader should evaluate each of these potential errors when applying our method.

1) H_2O although accounted for in our Mg thermometer (Eq. (1)), is not accounted for in the $T^*(F)$ relationships. The effect of H_2O is to decrease the solidus and increase the temperature interval over which melting occurs. Failure to account for H_2O would result in anomalously high apparent F for a given temperature. If H_2O were accounted for, we expect calculated Ps to increase and Ts to decrease (Fig. 9A). Thus, if H_2O is important, but unaccounted for, calculated Ps are minimum bounds and calculated Ts are maximum bounds. Peridotite residues that yield negative calculated Ps may thus be a sign that water was involved in melting.

2) All Fe is treated as Fe^{2+}. If the oxygen fugacity is unusually high during melting, the proportion of Fe in the melt that is Fe^{3+} is also high. Ignoring the contribution of Fe^{3+} in the melt, if significant ($>0.1Fe_T$), would result in over-estimation of P and T (Fig. 9A). However, for the most part, oxygen fugacity of the upper mantle is not oxidized enough for this to be a serious concern (Canil, 1997, 2002; Li and Lee, 2004; Frost and McCammon, 2008; Lee et al., 2010b).

3) Heterogeneity or secular change in Fe content of *source* mantle must also be considered (Fig. 9B). A mantle source anomalously rich in Fe results in higher calculated Ts and Ps. A mantle source depleted in Fe results in lower Ts and Ps. One issue is whether there has been a secular change in the bulk Fe and Mg content of the convecting mantle. It can easily be shown that progressive production and storage of oceanic/continental crust throughout Earth's history results in negligible change in the FeO and MgO content of the mantle, so such secular changes are probably not important. However, we cannot rule out the possibility of localized Fe-rich lithologies within the upper (Liu et al., 2008) or lower mantle (Francis et al., 1999) that may have contributed to the formation of cratonic mantle. If a high Fe source dominates for most of the cratonic peridotites, our currently estimated Ps and Ts are minimum bounds.

4) Metasomatic modification of residual peridotite compositions, as discussed in the previous section, must be evaluated (Fig. 9A). Cryptic metasomatism, wherein only trace elements are modified, does not pose a problem. However, any metasomatic processes that change Fe and Mg can lead to biases. For example, increases in Fe content without a change in Mg will yield low Ts and Ps. Some abyssal peridotites and Phanerozoic continental lithosphere peridotites can be Fe-rich (due to Fe metasomatism) for a given MgO content, resulting in low to even negative Ps. We also note that decreases in MgO without a concomitant decrease in FeO, such as what is commonly seen in the high temperature sheared peridotites from cratonic environments, yield high Ps and Ts. It is generally thought that these high temperature sheared peridotites represent highly melt-depleted peridotites that have been subsequently metasomatized (Boyd and Mertzman, 1987; Griffin et al., 1999; Lee et al., 2011). Finally, as discussed above, orthopyroxene-enrichment decreases Fe and Mg, resulting in over-estimation of P and T.

5) Serpentinization can lead to increases in Mg and decreases in Fe, as evidenced by the higher Mg# of serpentine minerals compared to that of their ultramafic protoliths. As shown in Fig. 9A, this would decrease estimated Ts and Ps. Thus, another explanation for why some ophiolitic, fore-arc and abyssal peridotites give negative Ps could be that their bulk compositions have been compromised by serpentinization.

5. Discussion: making cratons

The protoliths of cratonic peridotites appear to have formed at Ps lower and Ts higher than their final subsolidus equilibration Ps and Ts. This implies a net counter clockwise P–T path in which hot shallow cratonic peridotites increased in P and cooled. Of course, more than a billion years likely elapsed between the initial and final states, so it is not clear if this net P–T path reflects early craton stabilization or if the rocks experienced a more prolonged and tortuous P–T path, the evidence of which has all been erased by subsolidus re-equilibration. Regardless, a net counter clockwise P–T path is peculiar because as materials sink into the underlying

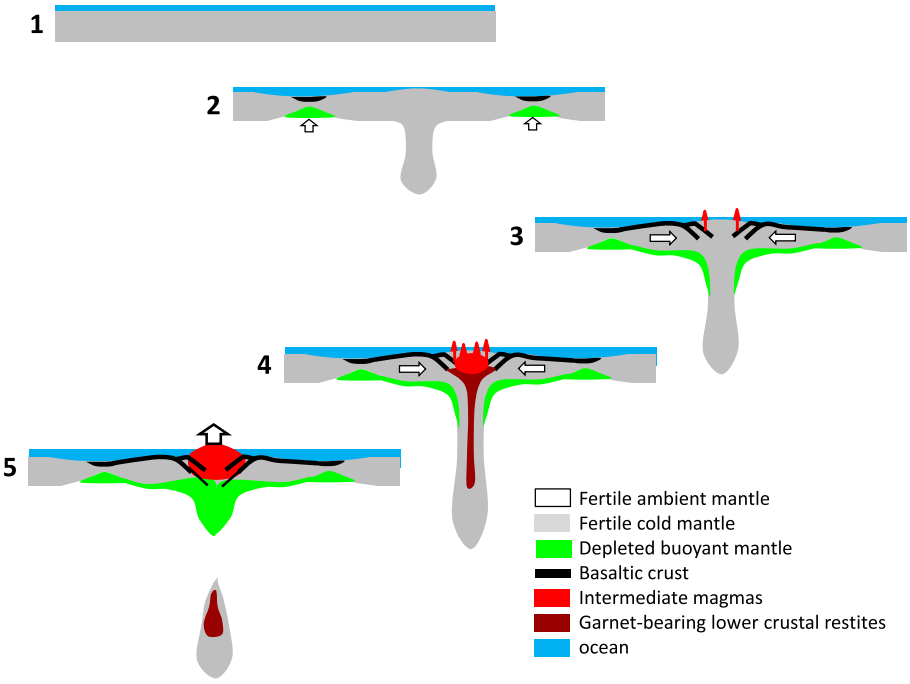

Fig. 10. Speculative conceptual cartoon of how thick cratonic mantle forms. 1) Initial state represents a stagnant lid condition, wherein the surface of the mantle is defined by a cold thermal boundary layer, which may or may not be melt-depleted. 2) A convective downwelling initiates, resulting in thickening of the boundary layer above the downwelling and thinning of the boundary layer in the far field. Beneath the thinning regime, mantle upwells and partially melts, generating low density, depleted peridotite residues and basaltic crust. 3) Continued downwelling draws the newly formed depleted mantle and basaltic crust towards the zone of convergence, resulting in thickened crust and mantle. Hydrothermally altered basaltic crust is underthrusted and begins to melt. 4) As crustal melting proceeds, felsic intermediate magmas rise to make the buoyant continental crust, leaving behind dense garnet-bearing crustal residues that founder along with any fertile peridotites. Melt-depleted peridotites (green) are too buoyant to founder. The end-product is a craton composed of a felsic crust and underlying mantle keel made of melt-depleted peridotites. (For interpretation of the references to color in this figure legend, the reader is referred to the web version of this article.)

hot mantle, they should heat up. For example, subducting slabs heat up and undergo prograde dehydration/melting reactions. The only tectonic environments in which cooling accompanied by an increase in P has been observed are in continent–continent collisions and ocean–continent subduction zones. For example, it is conceivable that the base of the upper plate in a thrust zone cools against the cold upper part of the underthrusting lower plate (Huerta et al., 1999). As an example of a counter-clockwise path in Phanerozoic ocean–continent subduction zones, Chin et al. (2012) showed that the arc crust and lithospheric mantle underwent rapid thickening followed by cooling as the arc lithosphere impinged upon the cold subducting slab. Chin et al. (2012, 2013) further showed that such thickening coincided with or was in response to increased magmatic flux and tectonic compression in the upper plate, suggesting that thickening of crust and lithospheric mantle may have been coupled with juvenile crust formation. Although this thickening process seen in Phanerozoic continental arcs may have no relevance to Archean craton formation, it does show that continental lithosphere can be stabilized by thickening or orogenic processes.

What types of thickening processes may have operated in the Archean? Some authors have argued that plate tectonics did not operate in the Archean: evidence for Phanerozoic-like subduction zones in the form of high P/low T metamorphism appears only in the Proterozoic (Stern, 2005). The potential T of the mantle in the Archean was likely hotter (1600–1800 °C) compared to 1300–1400 °C today (Nisbet et al., 1993; Abbott et al., 1994; Herzberg et al., 2007, 2010; Lee et al., 2009, 2010a), in which case, oceanic-type lithospheres might be thicker, more buoyant, and possibly stronger (owing to dehydration; Hirth and Kohlstedt, 1996; Korenaga, 2008) while basal lithospheric stresses are lower (due to lower viscosity mantle), altogether frustrating subduction and culminating in stagnant lid convection (Korenaga, 2006; O'Neill et al., 2007). Indeed, the apparent episodicity of continent formation (Condie, 1998) has been suggested to be a manifestation of Earth's convective system switching between stagnant lid and mobile lid (plate tectonics) regimes, the former characterized by quiescence and the latter by rapid continental crust formation (O'Neill et al., 2007).

We suggest a model (Fig. 10) that may be able to reconcile the above observations, with the caveat that any suggestions are clearly speculations. We assume that peaks in zircon age populations indicate preferential continental growth whereas time intervals without significant zircon age populations represent periods of minimal crustal growth rather than artifacts of sampling or preservation (Condie and Aster, 2010). We assume, for sake of argument, that these quiescent periods reflect a stagnant lid regime as discussed above. In a stagnant lid regime, the Earth's cold upper thermal boundary layer manifests itself as a one-plate lithosphere, that is, there is no lateral mobility of the plate, no plate boundaries and hence no subduction zones, transforms, or mid-ocean ridges. This does not mean that convective downwellings/upwellings are absent in a stagnant lid regime. Small-scale convective instabilities operate at the base of the upper thermal boundary layer and ultimately limit its thickness. However, O'Neill et al. (2007) showed that regions of downwelling result in thickening of the lithosphere whereas regions of upwelling thin the lithosphere. The combination of negative thermal buoyancy and increases in viscous forces eventually act to break the thermal boundary layer, initiating a focused, plate like downwelling, that is, a subduction zone. This results in rapid orogenic thickening, marking the transition from stagnant to mobile lid states (e.g., plate tectonics).

We suggest that large amounts of melt are extracted from the mantle in the upwelling zones, generating a thermal boundary layer composed of a thick basaltic crust and a lithospheric mantle composed of low pressure, high degree peridotite residues.

This crust–mantle package is rapidly transported laterally towards the zones of convergence. The basaltic crust, because of its low density, initially undergoes orogenic thickening rather than being subducted away deep into the mantle. The depleted peridotite is also chemically buoyant, and thus, instead of being dragged deep into the lower mantle by downward viscous forces, it generates a thickened mantle keel. We speculate that thickening of the basaltic crust causes the lower crust to heat up, owing to the high concentrations of radioactive heat producing elements (e.g., U and Th) in the basaltic crust billions of years ago (West and Mareschal, 1979; Rey et al., 2003; Sandiford et al., 2004). This heating results in extensive partial melting of the lower crust, generating intermediate magmas (tonalites, trondjhemites, and granodiorites) that rise to form the upper crust and leave behind garnet-rich restites at depth ("eclogite" *sensu lato*). We envision that the Earth's surface was already graced with water in the Archean, such that basalts formed at the upwelling zones become hydrothermally altered, hence anatexis in the orogenic thickening zones would involve partial melting of hydrated lithologies, such as amphibolites; such hydrous melting might generate magmas with trace element signatures similar to what is seen in modern subduction zones. We speculate that the ensuing intermediate melts that rise to the surface mark the first emergence of large continental landmasses because the low densities of these intermediate rocks buoy the crust above sea-level. This, of course, can only happen if the dense garnet-rich restites can be removed. We suggest that these garnet-rich restites, along with any fertile mantle, sink through the forming cratonic mantle root (cf. Herzberg et al., 1983; Arndt and Goldstein, 1989; Kay and Kay, 1993; Rudnick, 1995; Ducea, 2002; Lee et al., 2006; Jagoutz and Schmidt, 2012; Lee, 2014). Inherent in our model is the assumption that the building blocks of the cratonic mantle root were still relatively hot, and hence of low enough viscosity for the garnet-rich rocks to sink through. The final product is a continent composed of a felsic crust and a melt-depleted mantle keel. Our model has various elements in common with other models (Rollinson, 1997; Foley et al., 2002, 2003; Rapp et al., 2003; Smithies et al., 2003; Condie, 2005; Bedard, 2006). Given the speculative nature of all these models, especially ours, there is no pressing need to compare and contrast them. The reader should evaluate the merits of these models and ours from his/her own perspective and experience.

6. Conclusions

The Ps and Ts at which cratonic peridotites melted, that is, their igneous protolith conditions, are lower and higher, respectively, than their subsolidus/metamorphic Ps and Ts. The building blocks of cratonic peridotites formed by high degree melting at depths between 30 and 150 km and potential temperatures between 1450 and 1750 °C. After their formation, the peridotites were transported to depths of 120–200 km and cooled. These observations support hypotheses that invoke orogenic processes in the formation of cratons.

Acknowledgements

This work was conceived in bits and spurts beginning in 2010. Preliminary work was first presented at the 2012 International Geologic Conference in Sydney, Australia, but was not completed until fall 2013 in preparation for a special session on continental lithosphere led by Katie Cooper, Meghan Miller, and Heather Ford at the 2013 American Geophysical Union conference in San Francisco, California. Peter Luffi, Monica Erdman, and Michael Farner provided useful discussions/feedback. Claude Herzberg, Yaoling Niu, Dmitri Ionov, and Tim Elliot are thanked for detailed reviews and suggestions. This work was supported by the NSF (EAR-1119315).

Appendix A. Supplementary material

Supplementary material related to this article can be found online at http://dx.doi.org/10.1016/j.epsl.2014.06.048.

References

Abbott, D., Burgess, L., Longhi, J., Smith, W.H.F., 1994. An empirical thermal history of the Earth's upper mantle. J. Geophys. Res. 99.
Albarède, F., 1992. How deep do common basaltic magmas form and differentiate? J. Geophys. Res. 97, 10997–11009.
Armytage, R.M.G., Brandon, A.D., Peslier, A.H., Lapen, T.J., 2014. Osmium isotope evidence for early to middle Proterozoic mantle lithosphere stabilization and concomitant production of juvenile crust in Dish Hill, CA peridotite xenoliths. Geochim. Cosmochim. Acta 137, 113–133.
Arndt, N.T., Goldstein, S.L., 1989. An open boundary between lower continental–crust and mantle – its role in crustal formation and recycling. Tectonophysics 161, 201–212.
Asimow, P.D., Hirschmann, M.M., Stolper, E.M., 2001. Calculation of peridotite partial melting from thermodynamic models of minerals and melts, IV. Adiabatic decompression and the composition and mean properties of mid-ocean ridge basalts. J. Petrol. 42, 963–998.
Aulbach, S., 2012. Craton nucleation and formation of thick lithospheric roots. Lithos 149, 16–30.
Aulbach, S., Griffin, W.L., O'Reilly, S.Y., McCandless, T.E., 2004. Genesis and evolution of the lithospheric mantle beneath the Buffalo Head Terrane, Alberta (Canada). Lithos 77, 413–451.
Baker, M.B., Grove, M., Price, R., 1994. Primitive basalts and andesites from the Mt. Shasta region, N. California: products of varying melt fraction and water content. Contrib. Mineral. Petrol. 118, 111–129.
Beattie, P., 1993. Olivine-melt and orthopyroxene-melt equilibria. Contrib. Mineral. Petrol. 115, 103–111.
Bedard, J.H., 2006. A catalytic delamination-driven model for coupled genesis of Archaean crust and sub-continental lithospheric mantle. Geochim. Cosmochim. Acta 70, 1188–1214.
Bernstein, S., Kelemen, P.B., Hanghoj, K., 2007. Consistent olivine Mg# in cratonic mantle reflects Archean mantle melting to the exhaustion of orthopyroxene. Geology 35, 459–462.
Blatter, D.L., Carmichael, I.S.E., 2001. Hydrous phase equilibria of a Mexican high-silica andesite: a candidate for a mantle origin? Geochim. Cosmochim. Acta 65, 4043–4065.
Boyd, F.R., 1987. High- and low-temperature garnet peridotite xenoliths and their possible relation to the lithosphere–asthenosphere boundary beneath southern Africa. In: Nixon, P.H. (Ed.), Mantle Xenoliths. John Wiley & Sons Ltd, pp. 403–412.
Boyd, F.R., 1989. Compositional distinction between oceanic and cratonic lithosphere. Earth Planet. Sci. Lett. 96, 15–26.
Boyd, F.R., McAllister, R.H., 1976. Densities of fertile and sterile garnet peridotites. Geophys. Res. Lett. 3, 509–512.
Boyd, F.R., Mertzman, S.A., 1987. Composition and structure of the Kapvaal lithosphere, Southern Africa. In: Mysen, B.O. (Ed.), Magmatic Processes: Physicochemical Principles: A Volume in Honor of Hatten S. Yoder, Jr. In: Geochem. Soc. Spec. Pub., pp. 13–24.
Boyd, F.R., Gurney, J.J., Richardson, S.H., 1985. Evidence for a 150–200 km thick Archean lithosphere from diamond inclusion thermobarometry. Nature 315, 387–389.
Boyd, F.R., Pokhilenko, N.P., Pearson, D.G., Mertzman, S.A., Sobolev, N.V., Finger, L.W., 1997. Composition of the Siberian cratonic mantle: evidence from Udachnaya peridotite xenoliths. Contrib. Mineral. Petrol. 128, 228–246.
Brey, G.P., Kohler, T., 1990. Geothermobarometry in four-phase lherzolites II. New thermobarometers, and practical assessment of existing thermobarometers. J. Petrol. 31, 1353–1378.
Bulatov, V.K., Girnis, A.V., Brey, G.P., 2002. Experimental melting of a modally heterogeneous mantle. Mineral. Petrol. 75, 131–152.
Canil, D., 1997. Vanadium partitioning and the oxidation state of Archaean komatiite magmas. Nature 389, 842–845.
Canil, D., 2002. Vanadium in peridotites, mantle redox and tectonic environments: Archean to present. Earth Planet. Sci. Lett. 195, 75–90.
Canil, D., 2004. Mildly incompatible elements in peridotites and the origins of mantle lithosphere. Lithos 77, 375–393.
Carlson, R., Irving, A.J., 1994. Depletion and enrichment history of subcontinental lithospheric mantle: an Os, Sr, Nd and Pb isotopic study of ultramafic xenoliths from the northwestern Wyoming Craton. Earth Planet. Sci. Lett. 126, 457–472.
Carlson, R.W., Pearson, D.G., Boyd, F.R., Shirey, S.B., Irvine, G., Menzies, A.H., Gurney, J.J., 1999. Re–Os systematics of lithospheric peridotites: implications for lithosphere formation and preservation. In: Gurney, J.J., Gurney, J.L., Pascoe, M.D., Richardson, S.R. (Eds.), Proc. VIIth International Kimberlite Conference, B.J. Dawson Volume, pp. 99–108.

Carlson, R.W., Pearson, D.G., James, D.E., 2005. Physical, chemical, and chronological characteristics of continental mantle. Rev. Geophys. 43, RG1001.
Chesley, J.T., Rudnick, R.L., Lee, C.-T., 1999. Re–Os systematics of mantle xenoliths from the East African Rift: age, structure, and history of the Tanzanian craton. Geochim. Cosmochim. Acta 63, 1203–1217.
Chin, E.J., Lee, C.-T.A., Luffi, P., Tice, M., 2012. Deep lithospheric thickening and refertilization beneath continental arcs: case study of the *P*, *T* and compositional evolution of peridotite xenoliths from the Sierra Nevada, California. J. Petrol. 53, 477–511.
Chin, E.J., Lee, C.-T.A., Tollstrup, D.L., Xie, L.-W., Wimpenny, J.B., Yin, Q.Z., 2013. On the origin of hot metasedimentary quartzites in the lower crust of continental arcs. Earth Planet. Sci. Lett. 361, 120–133.
Chin, E.J., Lee, C.-T.A., Barnes, J., 2014. Thickening, refertilization, and the deep lithosphere filter in continental arcs: constraints from major and trace elements and oxygen isotopes. Earth Planet. Sci. Lett. 397, 184–200.
Condie, K.C., 1998. Episodic continental growth and supercontinents: a mantle avalanche connection. Earth Planet. Sci. Lett. 163, 97–108.
Condie, K.C., 2005. TTGs and adakites: are they both slab melts? Lithos 80, 33–44.
Condie, K.C., Aster, R.C., 2010. Episodic zircon age spectra of orogenic granitoids: the supercontinent connection and continental growth. Precambrian Res. 180, 227–236.
Cooper, C.M., Lenardic, A., Levander, A., Moresi, L., 2006. Creation and preservation of cratonic lithosphere: seismic constraints and geodynamic models. In: American Geophysical Union Monograph, vol. 164, pp. 75–88.
Dodge, F.C.W., Lockwood, J.P., Calk, L.C., 1988. Fragments of the mantle and crust beneath the Sierra Nevada batholith: xenoliths in a volcanic pipe near Big Creek, California. Geol. Soc. Am. Bull. 100, 938–947.
Doucet, L.S., Ionov, D.A., Golovin, A.V., Pokhilenko, N.P., 2012. Depth, degrees and tectonic settings of mantle melting during craton formation: inferences from major and trace element compositions of spinel harzburgite xenoliths from the Udachnaya kimberlite, central Siberia. Earth Planet. Sci. Lett. 359–360, 206–218.
Draper, D.S., Johnston, A.D., 1992. Anhydrous PT phase relations of an Aleutian high-MgO basalt: an investigation of the role of olivine–liquid reaction in the generation of arc high-alumina basalts. Contrib. Mineral. Petrol. 112, 501–519.
Ducea, M.N., 2002. Constraints on the bulk composition and root foundering rates of continental arcs: a California arc perspective. J. Geophys. Res. 107. http://dx.doi.org/10.1029/2001JB000643.
Ducea, M.N., Saleeby, J.B., 1996. Buoyancy sources for a large, unrooted mountain range, the Sierra Nevada, California: evidence from xenolith thermobarometry. J. Geophys. Res. 101, 8229–8244.
Ducea, M.N., Saleeby, J.B., 1998. The age and origin of a thick mafic–ultramafic keel from beneath the Sierra Nevada batholith. Contrib. Mineral. Petrol. 133, 169–185.
Ehrenberg, S.N., 1982. Petrogenesis of garnet lherzolite and megacrystalline nodules from the Thumb, Navajo volcanic field. J. Petrol. 23, 507–547.
Ellis, D.J., Green, E.H., 1979. An experimental study of the effect of Ca upon garnet–clinopyroxene Fe–Mg exchange equilibria. Contrib. Mineral. Petrol. 66, 13–22.
Falloon, T.J., Danyushevsky, L.V., 2000. Melting of refractory mantle at 1.5, 2, and 2.5 GPa under anhydrous and H_2O-undersaturated conditions: implications for the petrogenesis of high-Ca boninites and the influence of subduction components on mantle melting. J. Petrol. 41, 257–283.
Falloon, T.J., Green, D.H., Danyushevsky, L.V., Faul, U.H., 1999. Peridotite melting at 1.0 and 1.5 GPa: an experimental evaluation of techniques using diamond aggregates and mineral mixes for determination of near-solidus melts. J. Petrol. 40, 1343–1375.
Falloon, T.J., Danyushevsky, L.V., Green, D.H., 2001. Peridotite melting at 1 GPa: reversal experiments on partial melt compositions produced by peridotite–basalt sandwich experiments. J. Petrol. 42, 2363–2390.
Feig, S.T., Koepke, J., Snow, J.E., 2006. Effect of water on tholeiitic basalt phase equilibria: an experimental study under oxidizing conditions. Contrib. Mineral. Petrol. 152, 611–638.
Foley, S.F., Tiepolo, M., Vannucci, R., 2002. Growth of early continental crust controlled by melting of amphibolite in subduction zones. Nature 417, 837–840.
Foley, S.F., Buhre, S., Jacob, D.E., 2003. Evolution of the Archaean crust by delamination and shallow subduction. Nature 421, 249–252.
Francis, D., Ludden, J., Johnstone, R., Davis, W., 1999. Picrite evidence for more Fe in Archean mantle reservoirs. Earth Planet. Sci. Lett. 167, 197–213.
Frost, D.J., McCammon, C.A., 2008. The redox state of Earth's mantle. Annu. Rev. Earth Planet. Sci. 36, 389–420.
Gaetani, G.A., Grove, T.L., 1998. The influence of water on melting of mantle peridotite. Contrib. Mineral. Petrol. 131, 323–346.
Gibson, S.A., Malarkey, J., Day, J.A., 2008. Melt depletion and enrichment beneath the western Kaapvaal craton: evidence from Finsch peridotite xenoliths. J. Petrol. 49, 1817–1852.
Gibson, S.A., McMahon, S.C., Day, J.A., Dawson, J.B., 2013. Highly refractory lithospheric mantle beneath the Tanzanian craton: evidence from Lashaine pre-metasomatic garnet-bearing peridotites. J. Petrol. 54, 1503–1546.
Griffin, W.L., O'Reilly, S.Y., 2007. Cratonic lithospheric mantle: is anything subducted? Episodes 30, 43–53.
Griffin, W.L., Cousens, D.R., Ryan, C.G., Suter, G.F., 1989. Ni in chrome garnet: a new geothermometer. Contrib. Mineral. Petrol. 103, 199–202.
Griffin, W.L., O'Reilly, S.Y., Ryan, C.G., 1999. The composition and origin of subcontinental lithospheric mantle. In: Mantle Petrology: Field Observations and High Pressure Experimentation: A Tribute to R. (Joe) Boyd. Geochemical Society, pp. 13–45.
Griffin, W.L., O'Reilly, S.Y., Abe, N., Aulbach, S., Davies, R.M., Pearson, N.J., Doyle, B.J., Kivi, K., 2003. The origin and evolution of Archean lithospheric mantle. Precambrian Res. 127, 19–41.
Grove, T.L., Juster, T.C., 1989. Experimental investigations of low-Ca pyroxene stability and olivine–pyroxene-liquid equilibria at 1-atm in natural basaltic and andesitic liquids. Contrib. Mineral. Petrol. 103, 287–305.
Grove, T.L., Gerlach, D.C., Sando, T.W., 1982. Origin of calc-alkaline series lavas at Medicine Lake Volcano by fractionation, assimilation and mixing. Contrib. Mineral. Petrol. 80, 160–182.
Grove, T.L., Elkins-Tanton, L.T., Parman, S.W., Chatterjee, N., Müntener, O., Gaetani, G.A., 2003. Fractional crystallization and mantle-melting controls on calc-alkaline differentiation trends. Contrib. Mineral. Petrol. 145, 515–533.
Gung, Y., Panning, M., Romanowicz, B., 2003. Global anisotropy and the thickness of continents. Nature 422, 707–711.
Hanson, G.N., Langmuir, C., 1978. Modelling of major elements in mantle-melt systems using trace element approaches. Geochim. Cosmochim. Acta 42, 725–741.
Harley, S.L., Green, D.H., 1982. Garnet–orthopyroxene barometry for granulites and peridotites. Nature 300, 697–701.
Helmstaedt, H., Schulze, D.J., 1989. Southern African kimberlites and their mantle sample; implication for Archean tectonics and lithosphere evolution. In: Spec. Publ., Geol. Soc. Aust., vol. 14, pp. 358–368.
Herzberg, C., 1992. Depth and degree of melting of komatiites. J. Geophys. Res. 97, 4521–4540.
Herzberg, C.T., 1993. Lithosphere peridotites of the Kaapvaal craton. Earth Planet. Sci. Lett. 120, 13–29.
Herzberg, C., 1999. Phase equilibrium constraints on the formation of cratonic mantle. In: Fei, Y., Bertka, C.M., Mysen, B.O. (Eds.), Mantle Petrology, Field Observations and High Pressure Experimentation, a Tribute to Francis R. (Joe) Boyd. In: Geochem. Soc. Spec. Pub., pp. 241–257.
Herzberg, C., 2004. Geodynamic information in peridotite petrology. J. Petrol. 45, 2507–2530.
Herzberg, C., Asimow, P.D., 2008. Petrology of some oceanic island basalts: PRIMELT2.XLS software for primary magma calculation. Geochem. Geophys. Geosyst. 9.
Herzberg, C., O'Hara, M.J., 2002. Plume-associated ultramafic magmas of Phanerozoic age. J. Petrol. 43, 1857–1883.
Herzberg, C., Rudnick, R.L., 2012. Formation of cratonic lithosphere: an integrated thermal and petrological model. Lithos 149, 4–15. http://dx.doi.org/10.1016/j.lithos.2012.01.010.
Herzberg, C., Zhang, J., 1996. Melting experiments on anhydrous peridotite KLB-1: compositions of magmas in the upper mantle and transition zone. J. Geophys. Res. 101, 8271–8295.
Herzberg, C.T., Fyfe, W.S., Carr, M.J., 1983. Density constraints on the formation of the continental Moho and crust. Contrib. Mineral. Petrol. 84, 1–5.
Herzberg, C., Asimow, P.D., Arndt, N.T., Niu, Y., Lesher, C.M., Fitton, J.G., Cheadle, M.J., Saunders, A.D., 2007. Temperatures in ambient mantle and plumes: constraints from basalts, picrites and komatiites. Geochem. Geophys. Geosyst. 8. http://dx.doi.org/10.1029/2006GC001390.
Herzberg, C., Condie, K.C., Korenaga, J., 2010. Thermal history of the Earth and its petrological expression. Earth Planet. Sci. Lett. 292, 79–88.
Hirschmann, M.M., 2000. The mantle solidus: experimental constraints and the effects of peridotite composition. Geochem. Geophys. Geosyst. 1. http://dx.doi.org/10.1029/2000GC000070.
Hirth, G., Kohlstedt, D.L., 1996. Water in the oceanic upper mantle; implications for rheology, melt extraction and the evolution of the lithosphere. Earth Planet. Sci. Lett. 144, 93–108.
Huerta, A.D., Royden, L.H., Hodges, K.V., 1999. The effects of accretion, erosion and radiogenic heat on the metamorphic evolution of collisional orogens. J. Metamorph. Geol. 17, 349–366.
Ionov, D.A., Hofmann, A.W., 2007. Depth of formation of subcontinental off-craton peridotites. Earth Planet. Sci. Lett. 261, 620–634.
Ionov, D.A., Chanefo, I., Bodinier, J.-L., 2005. Origin of Fe-rich lherzolites and wehrlites from Tok, SE Siberia by reactive melt percolation in refractory mantle peridotites. Contrib. Mineral. Petrol. 150, 335–353.
Ionov, D.A., Doucet, L.S., Ashchepkov, I.V., 2010. Composition of the lithospheric mantle in the Siberian Craton: new constraints from fresh peridotites in the Udachnaya-East kimberlite. J. Petrol. 51, 2177–2210.
Iwamori, H., McKenzie, D., Takahashi, E., 1995. Melt generation by isentropic mantle upwelling. Earth Planet. Sci. Lett. 134, 253–266.
Jagoutz, O., Schmidt, M.W., 2012. The formation and bulk composition of modern juvenile continental crust: the Kohistan arc. Chem. Geol. 298–299, 79–96.
Jaupart, C., Mareschal, J.C., 1999. The thermal structure and thickness of continental roots. Lithos 48, 93–114.
Jordan, T.H., 1978. Composition and development of the continental tectosphere. Nature 274, 544–548.
Jordan, T.H., 1988. Structure and formation of the continental tectosphere. J. Petrol. 1988, 11–37.

Kay, R.W., Kay, S.M., 1993. Delamination and delamination magmatism. Tectonophysics 219, 177–189.
Kelemen, P.B., Dick, H.J.B., Quick, J.E., 1992. Formation of harzburgite by pervasive melt/rock reaction in the upper mantle. Nature 358, 635–641.
Kelemen, P.B., Hart, S.R., Bernstein, S., 1998. Silica enrichment in the continental upper mantle via melt/rock reaction. Earth Planet. Sci. Lett. 164, 387–406.
Kogiso, T., Hirose, K., Takahashi, E., 1998. Melting experiments on homogeneous mixtures of peridotite and basalt: application to the genesis of ocean island basalts. Earth Planet. Sci. Lett. 162, 45–61.
Kopylova, M.G., Russell, J.K., 2000. Chemical stratification of cratonic lithosphere; constraints from the northern Slave Craton, Canada. Earth Planet. Sci. Lett. 181, 71–87.
Kopylova, M.G., Russell, J.K., Cookenboo, H., 1998. Upper-mantle stratigraphy of the Slave Craton, Canada; insights into a new kimberlite province. Geology 26, 315–318.
Kopylova, M.G., Russell, J.K., Cookenboo, H., 1999a. Petrology of peridotite and pyroxenite xenoliths from Jericho Kimberlite; implications for the thermal state of the mantle beneath the Slave Craton, northern Canada. J. Petrol. 40, 79–104.
Kopylova, M.G., Russell, J.K., Cookenboo, H.O., 1999b. Mapping the lithosphere beneath the north central Slave Craton. In: Proceedings of the 7th International Kimberlite Conference, pp. 468–479.
Korenaga, J., 2006. Archean geodynamics and the thermal evolution of Earth. In: Geophys. Monogr., vol. 164, pp. 7–32.
Korenaga, J., 2008. Urey ratio and the structure and evolution of Earth's mantle. Rev. Geophys. 46. http://dx.doi.org/10.1029/2007RG000241.
Krogh Ravna, E., 2000. The garnet–clinopyroxene Fe^{2+}–Mg geothermometer: an updated calibration. J. Metamorph. Geol. 18, 211–219.
Laporte, D., Toplis, M.J., Seyler, M., Devidal, J.-L., 2004. A new experimental technique for extracting liquids from peridotite at very low degrees of melting: application to partial melting of depleted peridotite. Contrib. Mineral. Petrol. 146, 463–484.
Lee, C.-T.A., 2006. Geochemical/petrologic constraints on the origin of cratonic mantle. In: Benn, K., Mareschal, J.-C., Condie, K.C. (Eds.), Archean Geodynamics and Environments. In: American Geophysical Union Monograph. Washington, D.C., pp. 89–114.
Lee, C.-T.A., 2014. Physics and chemistry of deep continental crust recycling. In: Treatise on Geochemistry, vol. 4. Elsevier, pp. 423–456.
Lee, C.-T., Rudnick, R.L., 1999. Compositionally stratified cratonic lithosphere: petrology and geochemistry of peridotite xenoliths from the Labait Volcano, Tanzania. In: Gurney, J.J., Gurney, J.L., Pascoe, M.D., Richardson, S.R. (Eds.), Proc. VIIth International Kimberlite Conference, B.J. Dawson Volume, pp. 503–521.
Lee, C.-T., Yin, Q.-Z., Rudnick, R.L., Chesley, J.T., Jacobsen, S.B., 2000. Osmium isotopic evidence for Mesozoic removal of lithospheric mantle beneath the Sierra Nevada, California. Science 289, 1912–1916.
Lee, C.-T., Rudnick, R.L., Brimhall, G.H., 2001a. Deep lithospheric dynamics beneath the Sierra Nevada during the Mesozoic and Cenozoic as inferred from xenolith petrology. Geochem. Geophys. Geosyst. 2.
Lee, C.-T., Yin, Q., Rudnick, R.L., Jacobsen, S.B., 2001b. Preservation of ancient and fertile lithospheric mantle beneath the southwestern United States. Nature 411, 69–73.
Lee, C.-T.A., Brandon, A.D., Norman, M.D., 2003. Vanadium in peridotites as a proxy for paleo-fO_2 during partial melting: prospects, limitations, and implications. Geochim. Cosmochim. Acta 67, 3045–3064.
Lee, C.-T.A., Lenardic, A., Cooper, C.M., Niu, F., Levander, A., 2005. The role of chemical boundary layers in regulating the thickness of continental and oceanic thermal boundary layers. Earth Planet. Sci. Lett. 230, 379–395.
Lee, C.-T.A., Cheng, X., Horodyskyj, U., 2006. The development and refinement of continental arcs by primary basaltic magmatism, garnet pyroxenite accumulation, basaltic recharge and delamination: insights from the Sierra Nevada, California. Contrib. Mineral. Petrol. 151, 222–242.
Lee, C.-T.A., Luffi, P., Plank, T., Dalton, H.A., Leeman, W.P., 2009. Constraints on the depths and temperatures of basaltic magma generation on Earth and other terrestrial planets using new thermobarometers for mafic magmas. Earth Planet. Sci. Lett. 279, 20–33.
Lee, C.-T.A., Luffi, P., Hoink, T., Li, J., Dasgupta, R., Hernlund, J., 2010a. Upside-down differentiation and generation of a "primordial" lower mantle. Nature 463, 930–933.
Lee, C.-T.A., Luffi, P., Le Roux, V., Dasgupta, R., Albarede, F., Leeman, W.P., 2010b. The redox state of arc mantle using Zn/Fe systematics. Nature 468, 681–685.
Lee, C.-T.A., Luffi, P., Chin, E.J., 2011. Building and destroying continental mantle. Annu. Rev. Earth Planet. Sci. 39, 59–90.
Li, Z.-X.A., Lee, C.-T.A., 2004. The constancy of upper mantle fO_2 through time inferred from V/Sc ratios in basalts. Earth Planet. Sci. Lett. 228, 483–493.
Li, Z.-X.A., Lee, C.-T.A., 2006. Geochemical investigation of serpentinized oceanic lithospheric mantle in the Feather River Ophiolite, California: implications for the recycling rate of water by subduction. Chem. Geol. 235, 161–185.
Li, Z.-X.A., Lee, C.-T.A., Peslier, A.H., Lenardic, A., Mackwell, S.J., 2008. Water contents in mantle xenoliths from the Colorado Plateau and vicinity: implications for the rheology and hydration-induced thinning of continental lithosphere. J. Geophys. Res. 113.
Liu, Y., Gao, S., Kelemen, P., Xu, W., 2008. Recycled crust controls contrasting source compositions of Mesozoic and Cenozoic basalts in the North China craton. Geochim. Cosmochim. Acta 72, 2349–2376.
Luffi, P., Saleeby, J., Lee, C.-T.A., Ducea, M.N., 2009. Lithospheric mantle duplex beneath the central Mojave Desert revealed by xenoliths from Dish Hill, California. J. Geophys. Res. 114.
McDade, P., Blundy, J.D., Wood, B.J., 2003. Trace element partitioning on the Tinaquillo lherzolite solidus at 1.5 GPa. Phys. Earth Planet. Inter. 139, 129–147.
McDonough, W.F., Sun, S.-S., 1995. The composition of the Earth. Chem. Geol. 120, 223–253.
Mukhopadhyay, B., Manton, W.I., 1994. Upper mantle fragments from beneath the Sierra Nevada batholith-partial fusion, fractional crystallization and metasomatism in subduction-related ancient lithosphere. J. Petrol. 35, 1418–1450.
Nisbet, E.G., Cheadle, M.J., Arndt, N.T., Bickle, M.J., 1993. Constraining the potential temperature of the Archean mantle: a review of the evidence from komatiites. Lithos 30, 291–307.
Niu, Y., 2004. Bulk-rock major and trace element compositions of abyssal peridotites: implications for mantle melting, melt extraction and post-melting processes beneath mid-ocean ridges. J. Petrol. 45, 2423–2458.
O'Neill, H.S.C., 1981. The transition between spinel lherzolite and garnet lherzolite, and its use as a geobarometer. Contrib. Mineral. Petrol. 77, 185–194.
O'Neill, C., Lenardic, A., Moresi, L., Torsvik, T.H., Lee, C.-T.A., 2007. Episodic Precambrian subduction. Earth Planet. Sci. Lett. 262, 552–562.
O'Reilly, S.Y., Griffin, W.L., Djomani, Y.H., Morgan, P., 2001. Are lithospheres forever? Tracking changes in subcontinental lithospheric mantle through time. GSA Today 11, 4–10.
Parkinson, I.J., Pearce, J.A., 1998. Peridotites from the Izu–Bonin–Mariana forearc (ODP Leg 125): evidence for mantle melting and melt–mantle interaction in a supra-subduction zone setting. J. Petrol. 39, 1577–1618.
Parman, S.W., Grove, T.L., 2004. Harzburgite melting with and without H_2O: experimental data and predictive modeling. J. Geophys. Res. 109. http://dx.doi.org/10.1029/2003JB002566.
Pearson, D.G., Wittig, N., 2008. Formation of Archaean continental lithosphere and its diamonds: the root of the problem. J. Geol. Soc. Lond. 165, 895–914.
Pearson, D.G., Carlson, R.W., Shirey, S.B., Boyd, F.R., Nixon, P.H., 1995a. Stabilisation of Archaean lithospheric mantle: a Re–Os isotope study of peridotite xenoliths from the Kaapvaal craton. Earth Planet. Sci. Lett. 134, 341–357.
Pearson, D.G., Shirey, S.B., Carlson, R.W., Boyd, F.R., Pokhilenko, N.P., Shimizu, N., 1995b. Re–Os, Sm–Nd, and Rb–Sr isotope evidence for thick Archaean lithospheric mantle beneath the Siberian craton modified by multistage metasomatism. Geochim. Cosmochim. Acta 59, 959–977.
Pearson, D.G., Canil, D., Shirey, S., 2003. Mantle samples included in volcanic rocks: xenoliths and diamonds. In: Holland, H.D., Turekian, K.K. (Eds.), Treatise of Geochemistry. Elsevier, Oxford, pp. 171–275.
Pichavant, M., Mysen, B.O., Macdonald, R., 2002. Source and H_2O content of high-MgO magmas in island arc settings: an experimental study of a primitive calc-alkaline basalt from St. Vincent, Lesser Antilles arc. Geochim. Cosmochim. Acta 66.
Pickering-Witter, J., Johnston, A.D., 2000. The effects of variable bulk composition on the melting systematics of fertile peridotite assemblages. Contrib. Mineral. Petrol. 140, 190–211.
Pollack, H.N., 1986. Cratonization and thermal evolution of the mantle. Earth Planet. Sci. Lett. 80, 175–182.
Pollack, H.N., Chapman, D.S., 1977. On the regional variation of heat flow, geotherms, and lithospheric thickness. Tectonophysics 38, 279–296.
Putirka, K.D., 2005. Mantle potential temperatures at Hawaii, Iceland, and the mid-ocean ridge system, as inferred from olivine phenocrysts: evidence for thermally driven mantle plumes. Geochem. Geophys. Geosyst. 6. http://dx.doi.org/10.1029/2005GC000915.
Putirka, K.D., 2008. Thermometers and barometers for volcanic systems. Rev. Mineral. Geochem. 69, 61–120.
Rapp, R.P., Shimizu, N., Norman, M.D., 2003. Growth of early continental crust by partial melting of eclogite. Nature 425, 605–609.
Rey, P.F., Philippot, P., Thebaud, N., 2003. Contribution of mantle plumes, crustal thickening and greenstone blanketing to the 2.75–2.65 Ga global crisis. Precambrian Res. 127, 43–60.
Riter, J.C.A., Smith, D., 1996. Xenolith constraints on the thermal history of the mantle below the Colorado Plateau. Geology 24, 267–270.
Robinson, J.A.C., Wood, B.J., Blundy, J.D., 1998. The beginning of melting of fertile and depleted peridotite at 1.5 GPa. Earth Planet. Sci. Lett. 155, 97–111.
Rollinson, H.R., 1997. Eclogite xenoliths in West African kimberlites as residues from Archaean granitoid crust formation. Nature 389, 173–176.
Rudnick, R.L., 1995. Making continental crust. Nature 378, 571–578.
Rudnick, R.L., McDonough, W.F., Orpin, A., 1994. Northern Tanzanian peridotite xenoliths: a comparison with Kaapvaal peridotites and inferences of metasomatic reactions. In: Meyer, H.O.A., Leonardos, O.H. (Eds.), Kimberlites, Related Rocks and Mantle Xenoliths. In: CPRM Special Publication, pp. 336–353.
Rudnick, R.L., McDonough, W.F., O'Connell, R.J., 1998. Thermal structure, thickness and composition of continental lithosphere. Chem. Geol. 145, 395–411.

Saltzer, R.L., Chatterjee, N., Grove, T.L., 2001. The spatial distribution of garnets and pyroxenes in mantle peridotites: pressure–temperature history of peridotites from the Kaapvaal craton. J. Petrol. 42, 2215–2229.

Sandiford, M., van Kranendonk, M.J., Bodorkos, S., 2004. Conductive incubation and the origin of dome-and-keel structure in Archean granite–greenstone terrains: a model based on the eastern Pilbara. Tectonics 23.

Schwab, B.E., Johnston, A.D., 2001. Melting systematics of modally variable, compositionally intermediate peridotites and the effects of mineral fertility. J. Petrol. 42, 1789–1811.

Shirey, S.B., Harris, J.W., Richardson, S.R., Fouch, M.J., James, D.E., Cartigny, P., Deines, P., Viljoen, F., 2002. Diamond genesis, seismic structure, and evolution of the Kaapvaal–Zimbabwe craton. Science 297, 1683–1686.

Simon, N.S.C., Carlson, R.W., Pearson, D.G., Davies, G.R., 2007. The origin and evolution of the Kaapvaal cratonic lithospheric mantle. J. Petrol. 48, 589–625.

Smith, D., 2000. Insights into the evolution of the uppermost continental mantle from xenolith localities on and near the Colorado Plateau and regional comparisons. J. Geophys. Res. 2000, 16769–16781.

Smithies, R.H., Champion, D.C., Cassidy, K.F., 2003. Formation of Earth's early Archean continental crust. Precambrian Res. 127, 89–101.

Stern, R.J., 2005. Evidence from ophiolites, blueschists, and ultrahigh-pressure metamorphic terranes that the modern episode of subduction tectonics began in Neoproterozoic time. Geology 33, 557–560.

Stolper, E., 1980. A phase diagram for mid-ocean ridge basalts: preliminary results and implications for petrogenesis. Contrib. Mineral. Petrol. 74, 13–27.

Sugawara, T., 2000. Empirical relationships between temperature, pressure, and MgO content in olivine and pyroxene saturated liquid. J. Geophys. Res. 105, 8457–8472.

Takahashi, E., 1980. Melting relations of an alkali-olivine basalt to 30 kbar, and their bearing on the origin of alkali basalt magmas. Carnegie Institution of Washington Year Book 79, 271–276.

Walker, R.J., Carlson, R.W., Shirey, S.B., Boyd, F.R., 1989. Os, Sr, Nd, and Pb isotope systematics of southern African peridotite xenoliths: implications for the chemical evolution of subcontinental mantle. Geochim. Cosmochim. Acta 53, 1583–1595.

Walter, M.J., 1998. Melting of garnet peridotite and the origin of komatiite and depleted lithosphere. J. Petrol. 39, 29–60.

Walter, M.J., 1999. Melting residues of fertile peridotite and the origin of cratonic lithosphere. In: Fei, Y., Bertka, C.M., Mysen, B.O. (Eds.), Mantle Petrology: Field Observations and High Pressure Experimentation: A Tribute to Francis R. (Joe) Boyd. In: Geochem. Soc. Spec. Pub., pp. 225–239.

Walter, M.J., 2003. Melt extraction and compositional variability in mantle lithosphere. In: Carlson, R.W. (Ed.), The Mantle and Core. Elsevier–Pergamon, Oxford, pp. 363–394.

Wan, Z., Coogan, L.A., Canil, D., 2008. Experimental calibration of aluminum partitioning between olivine and spinel as a geothermometer. Am. Mineral. 93, 1142–1147.

Wasylenki, L.E., Baker, M.B., Kent, A.J.R., Stolper, E.M., 2003. Near-solidus melting of the shallow upper mantle: partial melting experiments on depleted peridotite. J. Petrol. 44, 1163–1191.

West, G.F., Mareschal, J.C., 1979. A model for Archean tectonism. Part I. The thermal conditions. Can. J. Earth Sci. 16, 1942–1950.

Wittig, N., Pearson, D.G., Webb, M., 2008. Origin of cratonic lithosphere mantle roots: a geochemical study of peridotites from the North Atlantic Craton, West Greenland. Earth Planet. Sci. Lett. 274, 24–33.

Xu, Y.-G., 2001. Thermo-tectonic destruction of the Archaean lithospheric keel beneath the Sino-Korean craton in China: evidence, timing and mechanism. Phys. Chem. Earth, Part A, Solid Earth Geod. 26, 747–757.